Late Mesozoic compressional to extensional tectonics in the Yiwulüshan massif, NE China and their bearing on the Yinshan-Yanshan orogenic belt: Part II: Anisotropy of magnetic susceptibility and gravity modeling

Wei Lin, Nicolas Charles, Yan Chen, Ken Chen, Michel Faure, Lin Wu, Fei Wang, Qiuli Li, Jun Wang, Qingchen Wang

Late Mesozoic compressional to extensional tectonics in the Yiwulüshan massif, NE China and their bearing on the Yinshan–Yanshan orogenic belt: Part II: Anisotropy of magnetic susceptibility and gravity modeling

- Wei Lin[a]
- Nicolas Charles[b]
- Yan Chen[b]
- Ke Chen[a]
- Michel Faure[b]
- Lin Wu[a]
- Fei Wang[a]
- Qiuli Li[a]
- Jun Wang[a]
- Qingchen Wang[a]

- [a] State Key Laboratory of Lithospheric Evolution, Institute of Geology and Geophysics, Chinese Academy of Sciences, P. O. Box 9825, Beijing 100029, China
- [b] Université d'Orléans, ISTO, UMR 7327, 1A rue de la Férollerie, 45071 Orléans, France

Abstract

Granitoids play an important role in deciphering both crustal growth and tectonic evolution of Earth. In the eastern end of the Yinshan–Yanshan belt of North China Craton, the Yiwulüshan massif is a typical region that presents the tectonic evolution features of this belt. Our field work on the host rocks has demonstrated two phases of opposite tectonics: compressional and extensional, however, the deformation is almost invisible in the intrusive rocks. To improve the understanding of the tectonic evolution of the Yiwulüshan massif and the Late Mesozoic tectonics of East Asia, a multidisciplinary study has been carried out. In this study, anisotropy of magnetic susceptibility (AMS) and gravity modeling have been applied on these Jurassic plutons (Lüshan, Jishilazi and Guanyindong), which intrude into the Yiwulüshan massif. According to laboratory measurements and microscopic observations on thin sections, the AMS of the Yiwulüshan massif is characterized by secondary fabrics, indicating that the intensive post solidus deformation has reset the (primary) magmatic magnetic fabrics. A relatively gentle NW dipping magnetic foliation has been identified with two distinct groups of magnetic lineations of N34°E and N335°E orientations, namely L_{M1} and L_{M2}, relatively. Gravity modeling reveals a southward thinning of the massif with a possible feeding zone rooted in the northern part of the massif. Integrating all results from structural observation, geochronological investigation, AMS measurement and gravity modeling, two tectonic phases have been identified in the Yiwulüshan massif, posterior to the Jurassic (180–160 Ma) magmatism in the Yinshan–Yanshan area. The early one concerns a Late Jurassic–Early Cretaceous (~ 141 Ma) compressional event with a top-to-the-south to southwest sense of shear. The second one shows an Early Cretaceous (~ 126 Ma) NW–SE ductile extensional shearing. At that time, sedimentary basins widened and Jurassic plutons started to be deformed under post solidus conditions. In fact, the NW–SE trend of the maximum stretching direction is a general feature of East Asian continent during Late Mesozoic.

Keywords

- North China Craton;
- Yinshan–Yanshan fold and thrust belt;
- Yiwulüshan massif;
- Anisotropy of magnetic susceptibility;
- Gravity modeling;
- Late Mesozoic tectonic evolution

1. Introduction

The Late Mesozoic–Cenozoic tectonics of East Asia is characterized by both continental-scale compressional and extensional tectonics ([Zhao, 1963], [Zhao, 1990], [Davis et al., 1998], [Davis et al., 2001], [Ritts et al., 2001], [Zhao et al., 2004] and [Zhang et al., 2011b]). These different events often make difficulties to understand the general tectonic framework and the mechanisms of the deformations in East Asia during this period. That is why geoscientists have paid great attention since about one century on the Mesozoic tectonics of East Asia (e.g. [Wong, 1929], [Davis et al., 1998], [Davis et al., 2001], [Ritts et al., 2001] and [Wu et al., 2008] and references therein). Though more and more recent scientific results can be found in both Chinese and international journals (e.g. [Traynor and Sladen, 1995], [Chough et al., 2000], [Mazukabzov et al., 2006], [Erdenetsogt et al., 2009], [Andryushchenko et al., 2010], [Chough and Sohn, 2010], [Metelkin et al., 2010] and [Daoudene et al., 2011]) and several national and international conferences have been organized on this topic, the tectonic evolution and geodynamics of the different tectonic events are still hotly debated (e.g. [Davis et al., 2001], [Darby and Ritts, 2002], [Liu et al., 2005], [Lin et al., 2007], [Lin et al., 2008], [Vergely et al., 2007], [Davis and Darby, 2010], [Liu et al., 2011] and [Zhang et al., 2011a]).

As one of major blocks in East Asia, the North China Craton (NCC) experienced a complex tectonic evolution from Neoarchean to Proterozoic (Zhai and Santosh, 2011 and references therein; Geng et al., 2012), and the Yinshan–Yanshan fold and thrust belt (Yinshan–Yanshan belt) may be considered as the most representative zone in the NCC to illustrate these Late Mesozoic–Cenozoic tectonics (Fig. 1; [Wong, 1929], [Zhao, 1963], [Davis et al., 1998], [Cui et al., 2002] and [Ritts et al., 2001]). The Yinshan–Yanshan fold and thrust belt is a highland extending for more than 1000 km east–westward at about 40°N of latitude from the west of the Tan–Lu fault to the west of Inner Mongolia along the northern part of the NCC (Fig. 1). Late Mesozoic to Cenozoic continental sedimentation, magmatism and widespread intracontinental deformation, including compression, extension, and strike-slip faulting, characterize the Yinshan–Yanshan belt ([Zhao, 1963], [Cui and Wu, 1997], [Davis et al., 1998], [Davis et al., 2001], [Zheng et al., 1998], [Ritts et al., 2001] and [Deng et al., 2004]). It is generally recognized that the compressional deformation occurred during the late Early Jurassic and mainly during the Late Jurassic–Early Cretaceous. But largely extensional tectonics succeeded since late Early Cretaceous at ca. 130–120 Ma ([Davis et al., 2001], [Lin et al., 2007], [Lin et al., 2008], [Lin et al., 2011a], [Davis and Darby, 2010] and [Wang et al., 2011]). However, there are several “exceptional” cases, for instance, extensional tectonics such as basins (e.g. Songliao Basin; Li et al., 1997) and Metamorphic Core Complexes (e.g. Linglong Metamorphic Core Complex; Charles et al., 2011) can be also observed during the Late Jurassic–Early Cretaceous what we considered as “compressional” period. Consequently, though previous publications on this subject may be retraced back to the twenties of the last century, two fundamental questions remain (Wong, 1929). At the scale of NCC, is there only one distinct deformation style (compression or extension) during one geological period? Does

only one geodynamic mechanism operate during one geological period? To decipher these questions, the Yiwulüshan massif offers a good target for a multidisciplinary study.

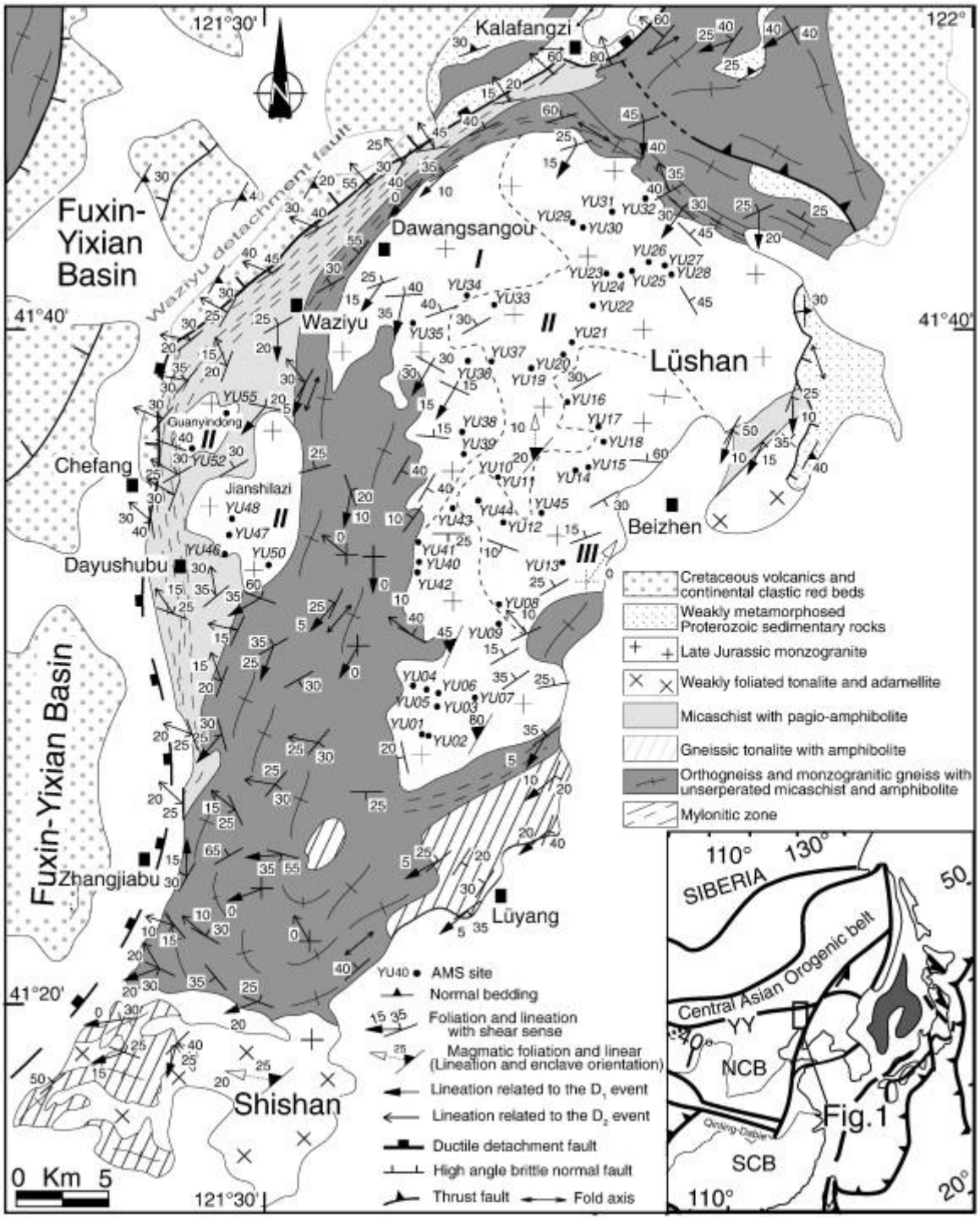

Fig. 1. Simplified geological map of the Yiwulüshan massif with AMS sampling sites position. The Lüshan pluton is subdivided into three petrographic domains: (I) Medium to fine-grained biotite granodiorite, (II) Medium to fine-grained biotite monzogranite and (III) Medium to fine-grained porphyritic biotite monzogranite.

The Yiwulüshan massif, located in the eastern end of the Yinshan–Yanshan belt and surrounded by Mesozoic–Cenozoic basins (Fig. 1), has experienced both compressional and extensional tectonics since Late Mesozoic (Lin et al., 2012). Though several studies dealing with structural geology and geochronology have recently focused on this area, the spatio-temporal tectonic evolution of the Yiwulüshan massif is still poorly demonstrated, especially in the view of polyphase deformations (e.g. [Ma et al., 1999], [Ma et al., 2000], [Zhang et al., 2002], [Darby et al., 2004] and [Lin et al., 2012] and references therein). Indeed, the Yiwulüshan massif has been described in literature as: (1) a Late Triassic or Jurassic to Cretaceous Metamorphic Core Complex ([LBGMR, Liaoning Bureau of Geology and Mineral Resources, 1989], [Lü and Liu, 1994], [Ma et al., 1999], [Ma et al., 2000], [Zhu et al., 2003] and [Darby et al., 2004]); (2) a massif exhibiting superimposed structures with a late Triassic dextral event followed by a Cretaceous extension, and a late sinistral strike-slip deformation (Zhang et al., 2002); and (3) a synkinematic pluton emplaced in an extensional setting (Liu et al., 2000). In order to better understand the tectonic evolution of the Yiwulüshan massif, a multidisciplinary study including structural geology, geochronology, anisotropy of magnetic susceptibility (AMS) and gravity modeling has been carried out. To present in detail numerous new results, this work is divided into two parts: Part I essentially concerns field structural observations and geochronological data (Lin et al., 2012, this issue), and this Part II shows AMS results and gravity modeling.

2. Geological setting and AMS sampling

The detailed geological descriptions and geochronological analyses are given in the companion paper (Lin et al., 2012, Part I), relevant summaries are only briefly described below.

2.1. Geological setting

In the eastern end of the Yinshan–Yanshan belt and to the west of the Tan–Lu fault, the Yiwulüshan massif is a typical region that presents the tectonic evolution features of the Yinshan–Yanshan belt (Fig. 1). Geometrically, the bulk architecture of the Yiwulüshan massif is dominated by a NNE–SSW elongated dome, which is bounded to the east by the NNE-trending Cretaceous to Eocene Xia–Liaohe basin (the northern part of Bohai Bay basin), and to the west by the Fuxin–Yixian Cretaceous graben basin (Fig. 1). Three main litho-tectonic units can be recognized in the Yiwulüshan massif from bottom to top: (1) a Neoarchean and Paleoproterozoic orthogneiss or gneissic monzogranite unit, which is considered as the basement rocks of the Yinshan–Yanshan belt ([LBGMR, Liaoning Bureau of Geology and Mineral Resources, 1989], [Ma et al., 1999] and [Zhang et al., 2002]); (2) a Paleoproterozoic plagioclase-amphibolite and micaschist unit ([LNBGMR-Yixian, 1970] and [LBGMR, Liaoning Bureau of Geology and Mineral Resources, 1989]); and (3) a Mesoproterozoic to Mesozoic sedimentary cover ([LNBGMR-Yixian, 1970], [Ma et al., 1999], [Ma et al., 2000] and [Zhu et al., 2003]). These three units are intruded by several generations of Mesozoic plutons.

The largest part of the Yiwulüshan massif is occupied by the 360 km^2 Lüshan biotite-monzogranitic pluton (Fig. 1). Two smaller monzogranitic plutons, named Jianshilazi and Guanyindong massifs, intruded the western part. Recent geochronological results on the Lüshan pluton and its country rocks indicate that the pluton was mainly emplaced during the middle to late Jurassic times ([Wu et al., 2006] and [Lin et al., 2012]). Geochemically, the Lüshan granitoids display compositional similarities to high-silica adakites described by Liu

et al. (2002). In the south and east of the Yiwulüshan massif, the medium to fine-grained tonalite and adamellite Shishan pluton crops out (Fig. 1). Petro-structural analysis coupled with recent ICP-MS zircon U/Pb dating at 123.0 ± 3.0 Ma (Wu et al., 2006) indicate that the Shishan pluton is an early Cretaceous syntectonic pluton.

The Lüshan pluton crops out in the central part of the Yiwulüshan massif. It has a NNE–SSW elongated elliptical-shape of ca. 35 × 12 km (Fig. 1). Petrologically, the pluton is composed of three units: (1) a medium to fine-grained biotite granodiorite (Unit I; Fig. 1); (2) a medium to fine-grained biotite monzogranite (Unit II; Fig. 1); and (3) a medium to fine-grained porphyritic biotite monzogranite (Unit III; Fig. 1). Muscovite monzogranite, two-mica granodiorite and garnet-bearing muscovite monzogranite could be also observed.

Unit I is located at the western part of the Lüshan pluton with a nearly N–S trending axis (Fig. 1). As mentioned in Part I, to the western boundary of this unit, the granodiorite is foliated with NE–SW trending mineral and stretching lineations with the moderate plunge (40–15°, Fig. 1). Amphibolite and micaschist xenoliths indicate also this NE–SW orientation. Well-developed foliation and lineation observed on its western margin decrease and then disappear inward in the pluton. Unit II occupies the central part of the Lüshan pluton with a N–S to NE–SW orientation. At the northern and southern ends of Unit II, the biotite monzogranite is foliated even mylonitized. This foliation weakens and then disappears inward in the pluton (Fig. 1). Similar to Unit II, Unit III is situated at the eastern part of the Lüshan pluton. Generally, most of this unit is undeformed, except for its eastern contact with gneiss and micaschist exhibiting a weak subhorizontal foliation (Fig. 1). It is worth to mention that boundaries between these three granitic units within the pluton are gradational and undeformed. Several authors previously had dated the Lüshan pluton. Su et al. (1994) first reported a zircon U/Pb age with a large error at 154 ± 18 Ma. Their data are not shown in Fig. 2 because the dated sample position was not indicated in their paper. Though several middle to late Jurassic ages (162–153 Ma) are available, but relatively inconsistent (Fig. 2; [Darby et al., 2004], [Wu et al., 2006], [Du et al., 2007], [Yin, 2007] and [Zhang et al., 2008]). Therefore, a new dating has been performed for this monzogranite with the highly precise Secondary Ion Mass Spectrometry (SIMS) method and gives a new age of 160.4 ± 1.8 Ma for the Lüshan pluton (Fig. 2; Lin et al., 2012).

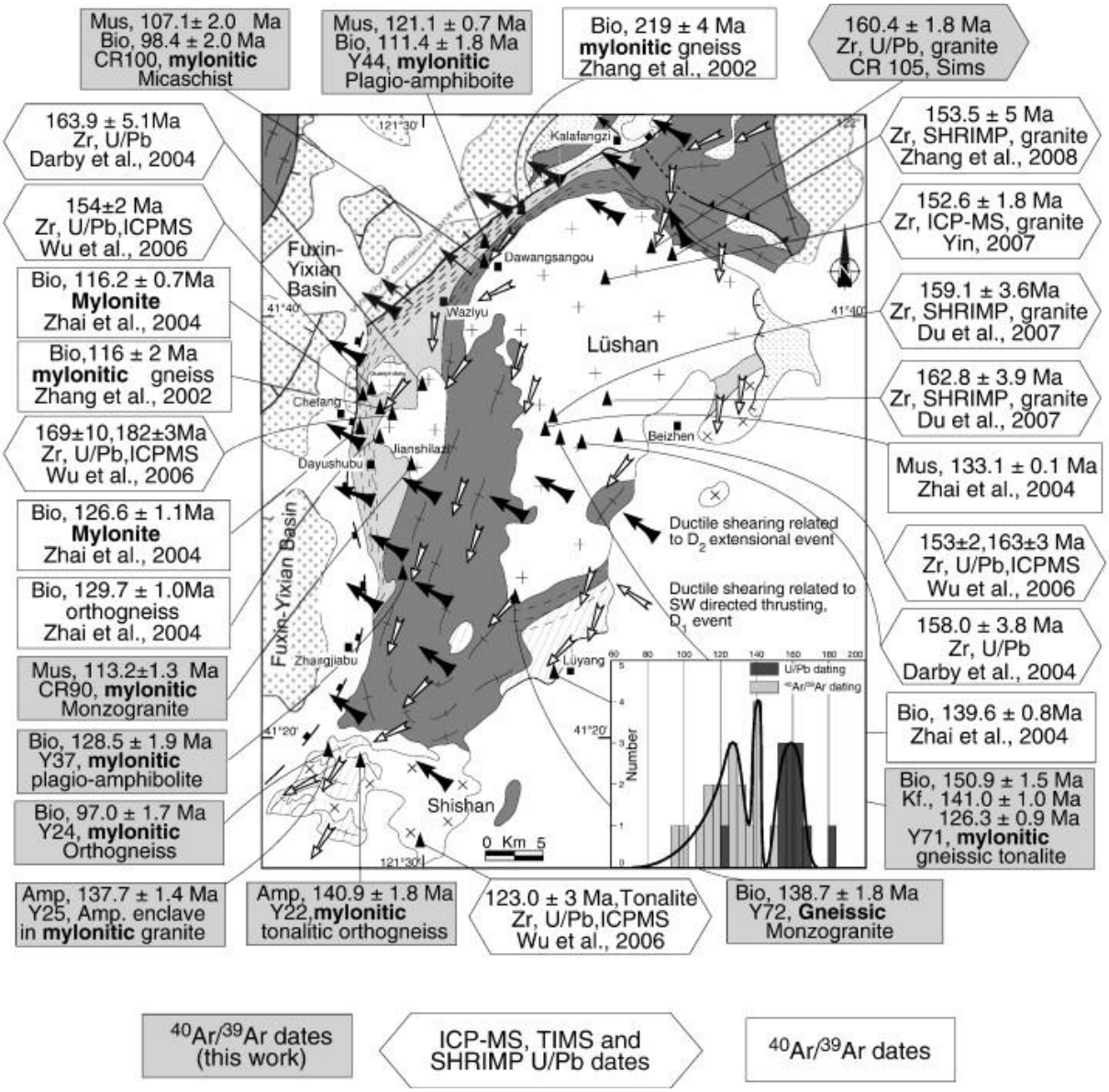

Fig. 2. Kinematic map of the Yiwulüshan massif with the compilation of available radiometric ages (figure captions are the same in Fig. 1). Age probability diagram of the Mesozoic igneous rocks is also shown. $^{40}Ar/^{39}Ar$ and U/Pb SIMS dating in gray color correspond to our work in Lin et al. (2012).

To the west of the Lüshan pluton, two smaller plutons (named Jianshilazi and Guanyindong) intruded the orthogneiss and micaschist (Fig. 1). These two plutons exhibit a weak NE-trending foliation. Close to the contact with the host-rock, a mylonitic zone associated with a NW dipping low angle foliation shows NW–SE mineral and stretching lineations with the weak plunge (average about 20°; Lin et al., 2012). Petrographically, these two plutons, composed of biotite monzogranite, are similar to Unit II of the Lüshan pluton (Fig. 1). The zircon U/Pb ages of the Jianshilazi and Guanyindong plutons range from 189 to 152 Ma like the Lüshan pluton (Fig. 2).

Structurally, tectonic fabrics cannot be observed everywhere due to the heterogeneity of deformation. However, according to our field observations, the tectonic features of the Yiwulüshan massif may be characterized by a general flat-lying to gently dipping foliation (Fig. 1). Four groups of deformation can be defined according to the style and the spatial distribution of lineations (see Part I for details, Lin et al., 2012). As an early deformation event, D_1 is expressed by the N–S to NE–SW mineral and stretching lineations with a top-to-the-south or southwest ductile shearing, interpreted as an early N–S to NE–SW compressional event (Lin et al., 2012). The regional geological understanding and available radiometric ages allow us to interpret this event as a Late Jurassic to Early Cretaceous south or southwest directed thrusting (Fig. 2). The subsequent three deformation events are related to the late extensional stages. D_2 is a ductile deformation characterized by a top-to-the NW sense of shear, related to the exhumation of the Yiwulüshan massif (Fig. 2). The age of this extensional event corresponds to the fast cooling period around 126 Ma according to the geochronological results from biotite and multi-domain diffusion of K-feldspar (Fig. 2; Lin et al., 2012). The following event D_3 corresponds to the development of recumbent folds formed along the two flanks, just after the exhumation stage D_2 of the massif. The youngest event, D_4, corresponds to normal brittle faulting which controlled the opening and infilling of the Cretaceous Fuxin–Yixian continental graben basin.

As mentioned above and shown in Part I, finite strain is not always visible in the field, particularly in the plutons, which intrude into the massif (Fig. 1; Lin et al., 2012). This may strongly mislead tectonic interpretations. Moreover, the only deformation traces related to the early D_1 phase have been observed within the massif. Nevertheless, it is evident that the massif has experienced also the later D_2 phase (Fig. 1). In order to obtain more representative results in both space and time, an anisotropy of magnetic susceptibility (AMS) study has been carried out in this massif.

2.2. AMS sampling

The AMS sampling has been carried out in the Lüshan, Jianshilazi and Guanyindong granitic plutons during two field campaigns in 2008 and 2009 with a relatively good geographic coverage (Table 1 and Fig. 1). A total of 302 oriented cores from 51 sites were sampled with a portable gasoline drill from the three different units of Lüshan, Jianshilazi, and Guanyindong plutons in the Yiwulüshan massif (Table 1). In average, six cores of about 4 to 6 cm in length are taken from each site which represents an about 10-meter-distance between two end cores. Cores were oriented with magnetic compass and, when it was necessary, solar one. The average difference between magnetic and solar declinations is about 8.4° ± 2.1°. Correction has been applied to the cores without solar orientation.

Table 1. The results of AMS measurements for the Lüshan, Jianshilazi and Guanyindong plutons. N: number of specimens. Dec, Inc, α_{95min}, α_{95max} are declination, inclination, Jelinek's statistic confidence at 95% level (Jelinek, 1981) in degrees, respectively. P_J: corrected anisotropy degree; T: anisotropy shape parameter; K_1: long axis of the AMS ellipsoid, represents the magnetic lineation and K_3: short axis of the AMS ellipsoid, is normal to the magnetic foliation.

	Coordinates					K1				K3			
	Latitude (°N)	Longitude (°E)	n	P_J	T	D (°)	I (°)	α_{95max}	α_{95min}	D (°)	I (°)	α_{95max}	α_{95min}
YU01	41.470	121.618	9	1.378	0.704	13.1	19.3	10.5	3.6	171.6	69.4	5.5	2.1
YU02	41.470	121.621	6	1.319	0.488	53.7	15.8	18.0	9.1	186.3	67.4	9.2	4.6
YU03	41.484	121.629	11	1.218	0.759	9.8	10.6	57.0	15.9	155.5	77.2	19.7	5.5
YU04	41.494	121.613	7	2.004	0.506	56.2	2.9	6.2	4.3	151.5	61.0	5.5	2.7
YU05	41.492	121.621	8	1.590	0.643	47.0	4.4	9.3	6.6	147.0	66.0	8.8	1.9
YU06	41.491	121.629	6	1.077	0.577	50.5	0.3	20.1	5.2	140.9	53.3	13.5	4.9
YU07	41.488	121.655	11	1.411	0.498	19.4	17.6	6.2	1.5	160.2	67.7	3.3	1.4
YU08	41.534	121.668	8	1.462	0.619	36.4	11.0	15.1	3.9	160.0	70.7	8.0	1.8
YU09	41.525	121.671	11	1.438	0.648	36.9	4.6	13.2	4.7	136.5	63.9	5.2	3.4
YU10	41.597	121.668	7	1.154	−0.278	5.0	27.4	21.4	8.9	183.3	62.6	15.5	10.9
YU11	41.597	121.668	5	1.353	0.303	17.8	10.2	21.2	2.1	133.5	67.3	12.5	2.4
YU12	41.575	121.674	10	1.412	0.294	5.7	9.4	9.1	3.7	127.8	72.8	9.5	3.7
YU13	41.556	121.716	9	1.590	0.483	29.9	4.0	11.8	2.6	136.6	76.4	4.7	2.7
YU14	41.602	121.724	8	1.399	0.798	342.4	5.7	20.2	4.0	173.5	84.2	7.4	3.3
YU15	41.603	121.733	8	1.091	0.158	8.5	15.6	14.4	4.7	127.6	60.2	8.9	4.5
YU16	41.635	121.715	7	1.247	0.406	300.0	36.8	15.8	4.3	154.3	47.9	11.1	3.5
YU17	41.623	121.740	8	1.212	0.536	20.1	8.3	13.3	1.9	129.4	66.1	5.2	3.1
YU18	41.616	121.744	13	1.167	−0.043	33.3	9.5	11.2	8.2	137.7	55.9	9.4	7.2
YU19	41.652	121.692	13	1.437	0.563	344.9	25.0	7.1	1.9	155.3	64.7	3.8	1.6
YU20	41.659	121.715	8	1.392	0.110	322.5	37.1	9.0	5.0	151.5	52.5	11.1	4.0
YU21	41.665	121.721	5	1.238	0.293	330.9	34.2	17.3	5.5	161.5	55.4	21.6	3.2
YU22	41.684	121.732	8	1.190	0.104	352.3	32.6	7.6	2.7	143.6	53.9	8.3	2.4
YU23	41.699	121.744	7	1.068	−0.045	332.6	19.2	32.3	9.9	232.5	26.7	18.8	11.1
YU24	41.698	121.754	8	1.252	0.102	355.5	24.1	40.7	6.9	238.7	45.2	15.1	5.6
YU25	41.700	121.763	9	1.098	0.808	339.9	24.1	63.6	3.0	172.3	65.4	7.2	5.0
YU26	41.705	121.774	11	1.157	0.139	307.8	22.5	11.9	7.0	179.5	56.1	14.9	6.5
YU27	41.704	121.786	7	1.160	−0.059	328.9	33.5	7.5	3.8	203.0	41.5	5.8	4.2
YU28	41.699	121.791	9	1.120	0.162	341.5	50.5	14.0	6.6	189.7	36.0	12.6	6.7
YU29	41.724	121.720	8	1.091	0.475	7.4	33.0	20.8	8.4	147.5	49.8	13.2	6.9
YU30	41.722	121.727	10	1.163	0.287	321.3	9.8	23.1	13.3	218.5	52.0	22.6	14.4
YU31	41.730	121.748	6	1.126	−0.153	3.9	28.5	30.6	17.1	169.7	60.8	20.6	18.1
YU32	41.736	121.771	9	1.031	0.287	126.7	10.9	37.3	3.9	227.2	43.6	7.7	2.3
YU33	41.683	121.665	12	1.433	0.829	15.9	28.5	19.7	2.3	154.2	54.0	2.8	1.8
YU34	41.686	121.647	7	1.285	0.703	6.1	34.1	21.0	2.5	157.2	52.2	6.7	2.5
YU35	41.673	121.608	7	1.042	0.386	3.1	23.9	9.3	6.2	142.4	59.7	9.4	5.8
YU36	41.655	121.647	8	1.035	0.656	51.2	16.3	52.3	16.6	174.2	61.8	21.5	15.3
YU37	41.655	121.661	10	1.525	0.523	11.8	30.3	18.2	6.8	165.3	56.8	9.1	6.2
YU38	41.620	121.644	10	1.373	0.453	5.6	14.6	10.5	2.2	150.7	72.3	4.6	2.1
YU39	41.609	121.645	12	1.323	0.522	27.1	4.3	8.7	2.7	126.8	66.0	4.0	2.1
YU40	41.555	121.614	11	1.167	0.270	19.8	19.6	11.2	6.4	188.5	70.1	8.1	4.4
YU41	41.564	121.610	10	1.338	0.179	37.7	9.1	13.5	3.6	183.6	79.0	10.2	3.8
YU42	41.550	121.613	10	1.239	0.260	43.7	5.4	11.0	5.5	143.5	61.1	8.5	4.8
YU43	41.582	121.638	5	1.369	0.462	41.7	10.4	6.9	0.7	186.4	77.4	9.8	3.3
YU44	41.586	121.656	11	1.056	0.379	180.1	0.7	11.3	6.4	272.2	72.6	7.5	3.6
YU45	41.580	121.701	8	1.374	0.751	24.8	9.6	39.0	5.4	157.0	75.8	6.0	4.2
YU46	41.555	121.467	10	1.050	0.604	189.5	13.7	25.8	2.7	60.3	68.9	13.4	2.5

	Coordinates					K1				K3			
	Latitude (°N)	Longitude (°E)	n	P_J	T	D (°)	I (°)	α_{95max}	α_{95min}	D (°)	I (°)	α_{95max}	α_{95min}
YU47	41.562	121.468	6	1.051	0.005	255.5	34.6	14.1	5.3	25.6	43.0	9.8	4.3
YU48	41.565	121.470	9	1.023	0.406	258.6	31.4	28.6	9.8	86.7	58.4	14.2	9.4
YU50	41.549	121.500	8	1.261	0.124	327.7	15.0	12.3	1.6	83.4	58.3	10.0	4.9
YU52	41.611	121.449	6	1.044	0.619	23.7	19.1	24.4	3.1	137.0	48.9	10.2	2.8
YU55	41.626	121.476	9	1.034	−0.472	44.5	4.5	24.0	6.5	173.7	82.9	35.2	9.3

3. Laboratory measurements

To identify the deformation state of sampled rocks, a petrofabric study has been performed with observation of thin-section due to a petrographic microscope.

Magnetic mineralogy investigations and AMS measurements have been made at the Institut des Sciences de la Terre d'Orléans (ISTO). Magnetic mineralogy was investigated by two methods: (1) thermomagnetic measurements performed with an AGICO KLY3-S Kappabridge susceptometer coupled with a CS3 furnace, and (2) measures of Isothermal Remanent Magnetization (IRM) within AGICO JR-5A automatic spinner magnetometer coupled with an ASC scientific magnetizer (model IM-10-30).

3.1. Petrofabric study

In order to recognize if the rocks experienced a significant deformation after their initial cooling or crystallization and then to define the origin(s) of magnetic fabrics (magmatic, and/or sub-solidus or post-solidus), micro-structural observations have been made on representative samples from both type of rocks, with good geographic distribution (Fig. 3 and Fig. 4). According to the strain amount, the mineral texture and grain size of quartz and biotite, three types of microstructures can be identified and described as follows.

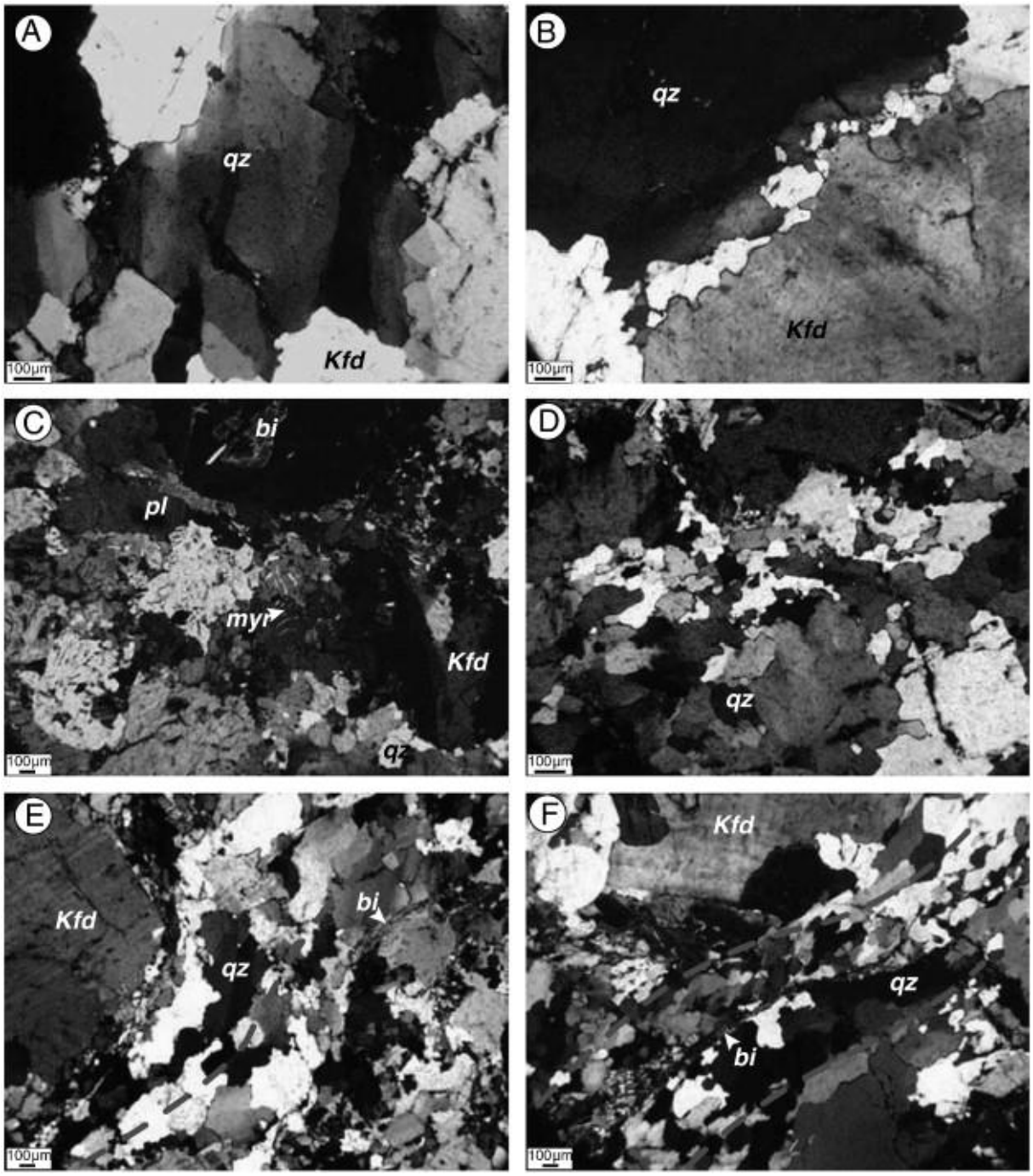

Fig. 3. Microphotographies of typical microstructures encountered within the Lüshan pluton. (A) and (B) Weak solid-state microstructures (site YU 18; E 121.74398°, N 41.6158°) with, chess-board quartz grains with undulose extinction, quartz grains with lobate borders. (C) and (D) Moderate solid-state microstructures with development of myrmekites (site YU 13, E 121.71612°, N 41.55588°) and recrystallized quartz grains (site YU 19, E 121.6918°, N 41.65178). (E) and (F) Strong solid-state microstructures with biotite foliation development and intensive quartz grains recrystallization (sites YU 01, E 121.61832°; N 41.47002° and YU 08, E 121.66843°; N 41.53384°); Kfd: potassium feldspar, qz: quartz, bi: biotite, pl: plagioclase, and myr: myrmekite.

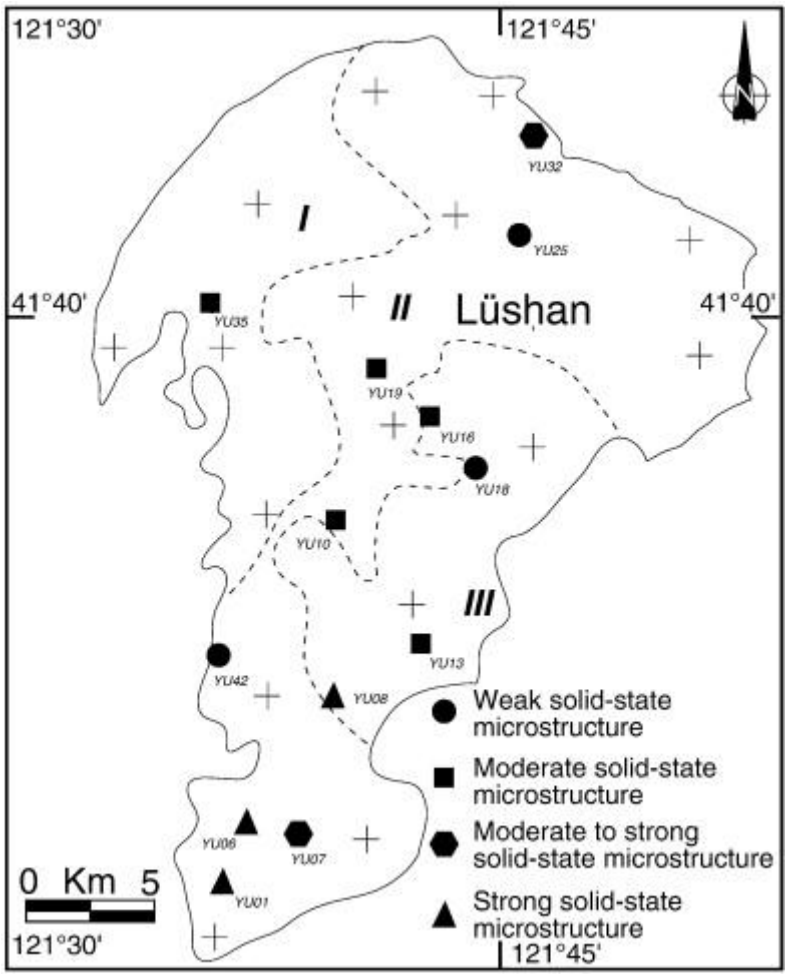

Fig. 4. Distribution map of the microstructures within the Lüshan pluton.

3.1.1. Weak solid-state fabric

Appearance of solid-state deformation in granitic rocks mainly depends on melt percentage shapes of minerals and their capacity to accommodate strain (Paterson et al., 1998). Thus, weak solid-state fabric is characterized by minerals, which are more deformed than those in the magmatically deformed rocks. In the weakly solid-state rocks, as a residual structure, minerals exhibit structures such as quartz grains partially replaced by subgrains with chessboard pattern and undulose extinction (Fig. 3A). Quartz grains boundaries are lobate or even slightly serrated (Fig. 3B). The beginning of dynamic recrystallization process is shown by the occurrence of new recrystallized and small-sized quartz grains development in some places. Biotite crystals become elongated and slightly kinked with bevel extinction. Feldspar grains present the undulose extinction and subhedral crystal habits with myrmekites. This microstructure indicates the solid-state flow deformation superposed on the magmatic structure at the central part of Lüshan massif where the post-solidus deformation was relatively weak (Fig. 1).

3.1.2. Moderate solid-state fabric

Moderate solid-state fabric is clearly shown by micro-structural evidences such as K-feldspars show microcline twinning and marginal replacement by myrmekite (Fig. 3C; [Eggleton and Buseck, 1980], [Bell and Johnson, 1989] and [Simpson and Wintsch, 1989]). Mosaic of quartz small-recrystallized grains (Fig. 3D) with serrated boundaries is typical of dynamic recrystallization, even if aggregates and recrystallized grains do not exhibit a mylonitic fabric. Combined brittle–ductile deformation is evidenced by the occurrence of fractured feldspars with quartz-filled veins. Elongated biotite crystals are kinked and internally deformed.

3.1.3. Strong solid-state fabric

Intense solid-state fabric is characterized by strongly recrystallized quartz grains organized in ribbons (Fig. 3E and F). Quartz and feldspar extremely fine-grained tails occur on residual phenocryst of K-feldspar. Biotite folium anastomoses around deformed porphyroclast of K-feldspar or plagioclase.

From the over view of the whole massif, even though the relative small numbers of observed thin-sections, an increasing tendency of deformation intensity could be indentified from the central part of the Lüshan pluton to margin (Fig. 4).

3.2. Magnetic mineralogy

Characterization of magnetic minerals, which carry magnetic susceptibility, is essential to understand the complex relationships between mineral grain shapes and orientations of rock fabrics (e.g. [Rochette et al., 1992] and [Tarling and Hrouda, 1993]). Magnetic investigation results of the Lüshan pluton are presented in Fig. 5 and Fig. 6.

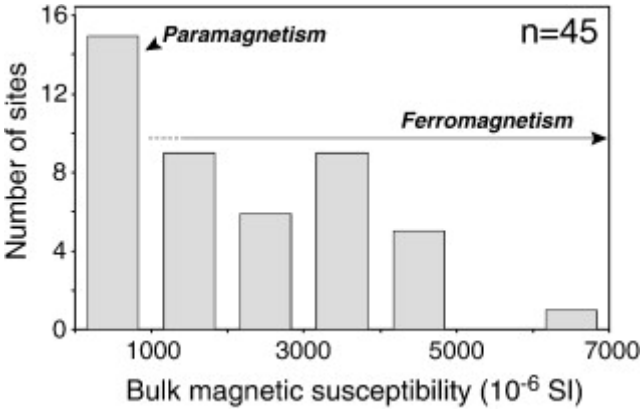

Fig. 5. Histogram of bulk magnetic susceptibility distribution for AMS sites of the Lüshan pluton.

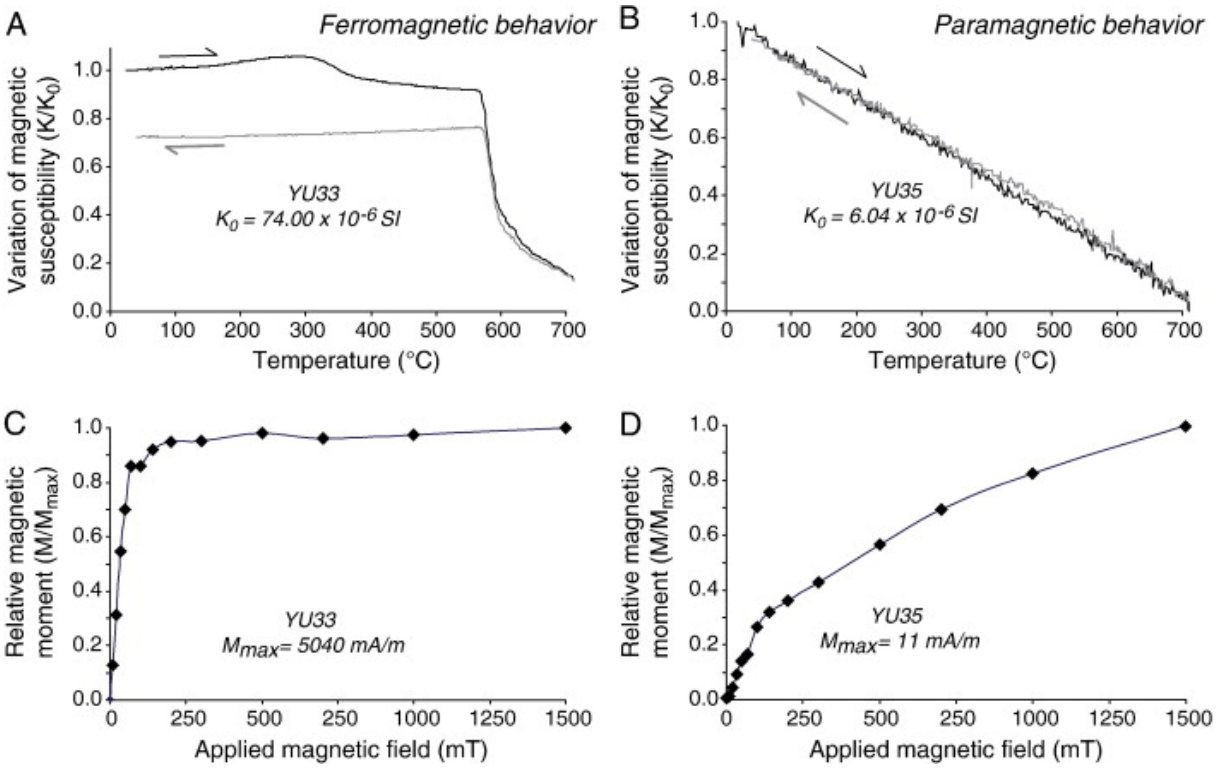

Fig. 6. Magnetic mineralogy investigations for the Lüshan, Jianshilazi and Guanyindong plutons. (A) and (B): Thermomagnetic measurements to determine Curie temperature; (C) and (D): Isothermal Remanent Magnetization (IRM) measurements.

The bulk magnetic susceptibility may qualitatively reveal the magnetic mineral property of studied rocks. Table 1 lists the average bulk magnetic susceptibility K_m for each measured site and Fig. 5 presents the histogram of K_m value distribution for the Lüshan pluton. K_m mainly varies from about 20 to 5000 × 10^{-6} SI, with one exceptional site of 6800 × 10^{-6} SI (Site 43; Table 1). Less than 30% of the sites shows K_m values lower than 1000 × 10^{-6} SI, implying that the paramagnetic minerals may be the main carriers of the magnetic susceptibility (e.g. Bouchez, 2000). More than 70% of the sites presents, however, K_m values higher than 1000 × 10^{-6} SI, suggesting the presence of ferromagnetic minerals. It may naturally relate the K_m variation to the type of sampled granites. However, this relation does not seem to be proved. Though the biotite monzogranite of Unit II includes most of higher K_m sites, such as Sites 43 and 33, many sites with weak K_m values also belong to the category of this type, such as Sites 6 and 32 (Table 1). This magnetic susceptibility heterogeneity may be related to the contamination of country rocks and/or mineral differentiation during the granite emplacement.

To better identify the magnetic carrier of the AMS collection, thermomagnetic experiments have been performed. Fig. 6A and B present representative results, showing typical ferromagnetic and paramagnetic behaviors, respectively. Fig. 6A reveals two relatively sharp drops of magnetic susceptibility at about 350 and 580 °C and a progressive drop from 600 to 680 °C. These drops may correspond to Curie temperatures of maghemite, magnetite and hematite, respectively. The relative consistency of heating and cooling paths shows the absence of mineralogical transformations during thermomagnetic experiments. Conversely, Fig. 6B shows a linear relationship between magnetic susceptibility and temperature, leading

us to consider the presence of paramagnetic minerals. According to Fig. 5, the majority of samples are ferromagnetic, instead of paramagnetic.

Measurements of Isothermal Remanent Magnetization (IRM) have been carried out on representative samples and Fig. 6C and D present typical curves of IRM acquisition for the rocks of the Lüshan pluton. The sample from Site 33, which has higher magnetic susceptibility value, is quickly saturated at about 150 mT with a high magnetic remanence of 5040 mA/m (Fig. 6C). This indicates the presence of soft coercitive minerals such as magnetite. In contrast, the sample from Site 35 with a lower magnetic susceptibility value shows a relatively rapid increase of magnetic susceptibility up to 150 mT and no saturation up to 1500 mT, with a very weak magnetic remanence of only 11 mA/m. This observation indicates that the mineral composition of weakly magnetic sites may be dominated by paramagnetic minerals, such as micas. As the high coercitive hematite seems not to be evidenced in this experiment, the hematite identified by the thermomagnetic experiment can be interpreted as newly transformed mineral during the heating instead of primary.

The good coherence between the bulk magnetic susceptibility measurement, thermomagnetic experiment and IRM acquisition reveals that the Lüshan granite has a bimodal magnetic mineralogy (Bouchez, 2000), dominated by ferromagnetic (magnetite, for the majority of sites) and paramagnetic (biotite and/or muscovite) minerals depending on sampling place in the massif. Fortunately, biotite and magnetite subfabric orientations exhibit no significant variations (Archanjo et al., 1995). Magnetic interactions between magnetite grains are negligible as shown by [Grégoire et al., 1995] and [Grégoire et al., 1998], which made AMS measurements usable with confidence.

3.3. Results of anisotropy of magnetic susceptibility (AMS) measurements

To avoid introducing the magnetic anisotropy by sample shapes, the cores have been cut into specimens of 2.2 cm in length and 2.5 cm in diameter of which is mostly close to a spherical shape. The AMS measurements were performed at low magnetic field (300 A/m) and the data processing was carried out according to the statistics described in [Jelinek, 1978] and [Jelinek, 1981]. The principal results are given in Table 1.

Three principal magnetic ellipsoidal axes have been calculated. The long axis (K_1 or K_{max}) corresponds to the magnetic lineation; the short one (K_3 or K_{min}) is the pole of the magnetic foliation defined by the ellipsoid section containing K_{max} and K_{int} (or K_2, intermediate axis; with $K_1 \geq K_2 \geq K_3$). According to Jelinek (1981), two parameters can be defined: (1) the shape parameter, $T = (2\eta_2 - \eta_1 - \eta_3) / (\eta_1 - \eta_3)$, varies between − 1 and + 1, and qualifies the shape of the ellipsoid (prolate when $T < 0$, or oblate when $T > 0$); and (2) the corrected anisotropy degree, $P_J = \{2[(\eta_1 - \eta_m)^2 + (\eta_2 - \eta_m)^2 + (\eta_3 - \eta_m)^2]\}^{1/2}$; where $\eta_1 = \ln K_1$, $\eta_2 = \ln K_2$, $\eta_3 = \ln K_3$ and $\eta_m = \sqrt[3]{\eta_1 * \eta_2 * \eta_3}$.

Only six out of total 51 sites show negative T values, representing a prolate shape of AMS ellipsoid (Fig. 7A and B; Table 1), and five of them drop in the granite of Unit II (biotite monzogranite; Table 1). This observation implies that the oblate shape dominates magnetic fabrics. In other words, magnetic foliation is statistically better defined compared to magnetic lineation. Calculated directions for each site are generally well-defined with confidence level (α_{95}) value-less than 20° (Table 1). The AMS collection is also characterized by rather strong anisotropy degree, with P_J values higher than 1.2 for the majority of sites (Table 1; Fig. 7A and C). This seems to indicate that the analyzed rocks may have experienced significant post-

solidus deformations (Tarling and Hrouda, 1993). It seems that no obvious correlation may be drawn between T, P_J and K_m (Fig. 7), which may imply that the variations of T and P_J are independent from the magnetic mineral composition according to Borradaile and Henry (1997).

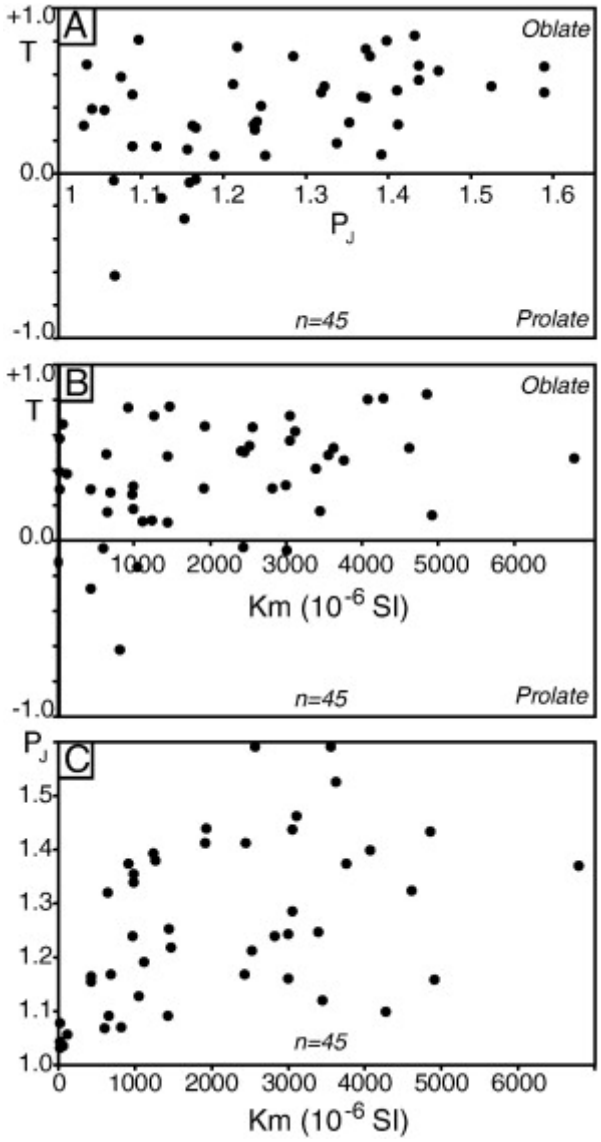

Fig. 7. AMS scalar parameters for the Lüshan pluton. (A) T (shape parameter) vs. P_J (corrected anisotropy degree), (B) T (shape parameter) vs. K_m (mean bulk magnetic susceptibility in 10^{-6} SI) and (C) P_J (corrected anisotropy degree) vs. K_m (mean bulk magnetic susceptibility in 10^{-6} SI). The calculations of T and P_J can be found in Jelinek (1981).

Fig. 8 presents equal-area projection of AMS results for each site of the Lüshan pluton within the Yiwulüshan massif. Squares and circles stand for K_1 (magnetic lineation) and K_3 (pole of magnetic foliation), respectively. Confidence ellipses at 95% level are drawn around site-mean direction. Bingham (1964) bimodal statistic method has been applied to the directional calculation of three principal AMS axes which produces maximal (α_{95max}) and minimal (α_{95min}) radiuses (Table 1; see also Le Goff et al. (1992) for detail statistic calculation). Globally, as described above, the magnetic foliations are statistically well-defined with low α_{95} values (Table 1 and Fig. 9A). Magnetic foliations are sub-horizontal and dip to the north to northwest, except for some sites located to the northeast corner of the massif, such as Sites 32, 24, 27, and 28 (Fig. 8 and Fig. 9A). These exceptions may be due to the border effect of the massif, i.e. magnetic foliations have been strongly influenced by the contact with country rocks during the pluton emplacement. Though magnetic lineations are statistically less grouped with respect to magnetic foliations and poorly defined at a few sites, such as Sites 25, 32, and 36, two sub-populations of directions may be recognized. The first major group includes most of the sites (more than 2/3 of the collection) with a weakly inclined and N–S to NNE–SSW dipping direction, such as Sites 1, 10, 15, 19, 29, 35, and 40 (Fig. 8 and Fig. 9A). Another minor group reveals a weakly inclined and NW–SE oriented magnetic lineation, such as Sites 14, 16, 21, 20, 24, 27, and 28. The first group covers almost all the pluton surface, except for its northeastern part occupied by the second and minor group (Fig. 8 and Fig. 9A). The density contour diagrams (Fig. 9B), calculated for individual AMS axes without orthogonal constraint in the three axes (Borradaile and Gauthier, 2003), reinforce previous observations. It is worthy to note that orientation of the magnetic fabrics seems consistent with tectonic ones measured in the field (Fig. 10) and, however, independent from the granite types, but probably related to the geographic position of sampling sites within the massif (see possible explanation in the Discussion).

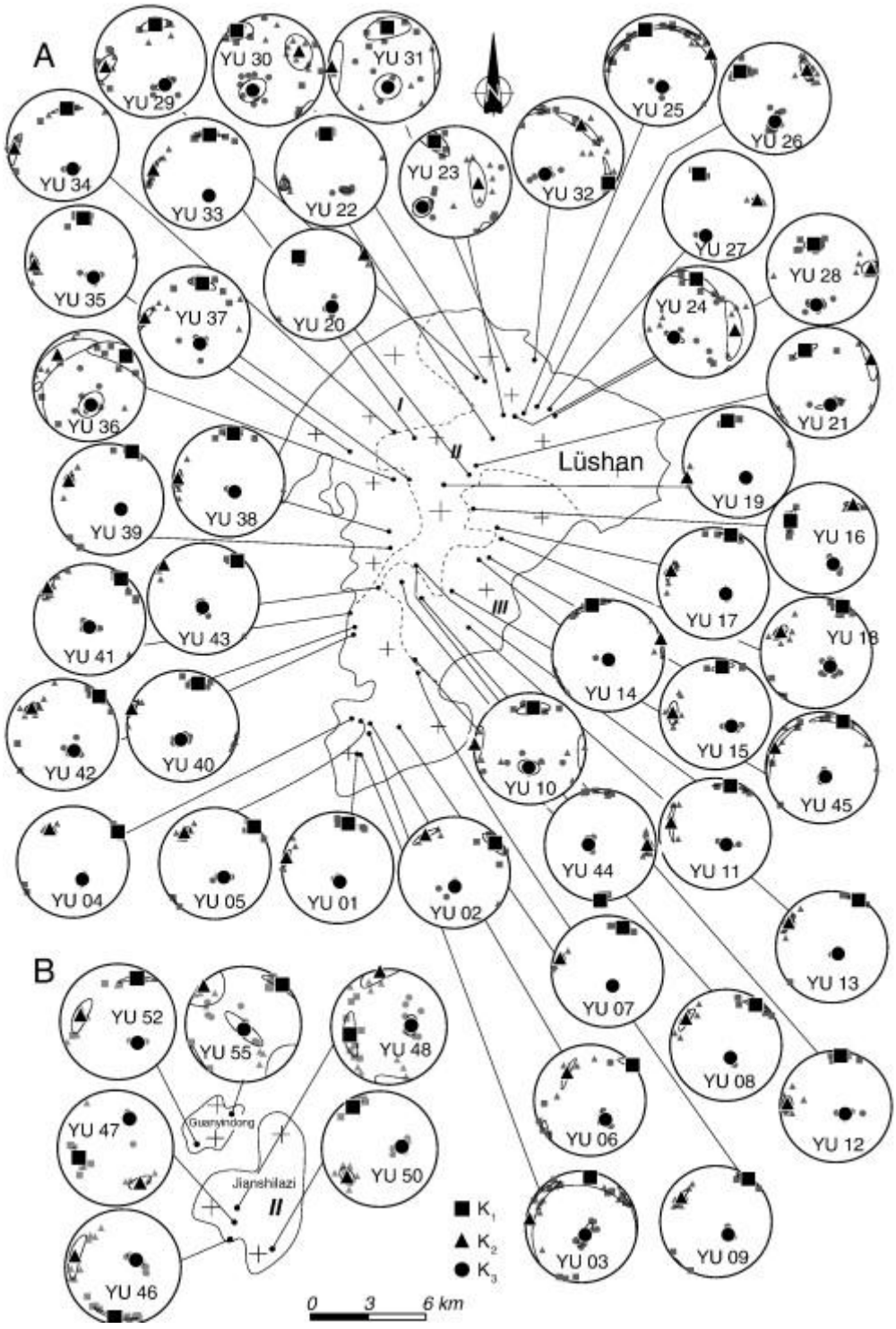

Fig. 8. Equal-area projection of AMS results for each site of (A) the Lüshan pluton and (B) Jianshilazi and Guanyindong plutons. Squares and circles stand for K_1 (magnetic lineation) and K_3 (pole of foliation), respectively. Small gray dots and larger black ones represent individual specimen and site-mean direction, respectively. Confidence ellipses at 95% level are drawn around site-mean direction.

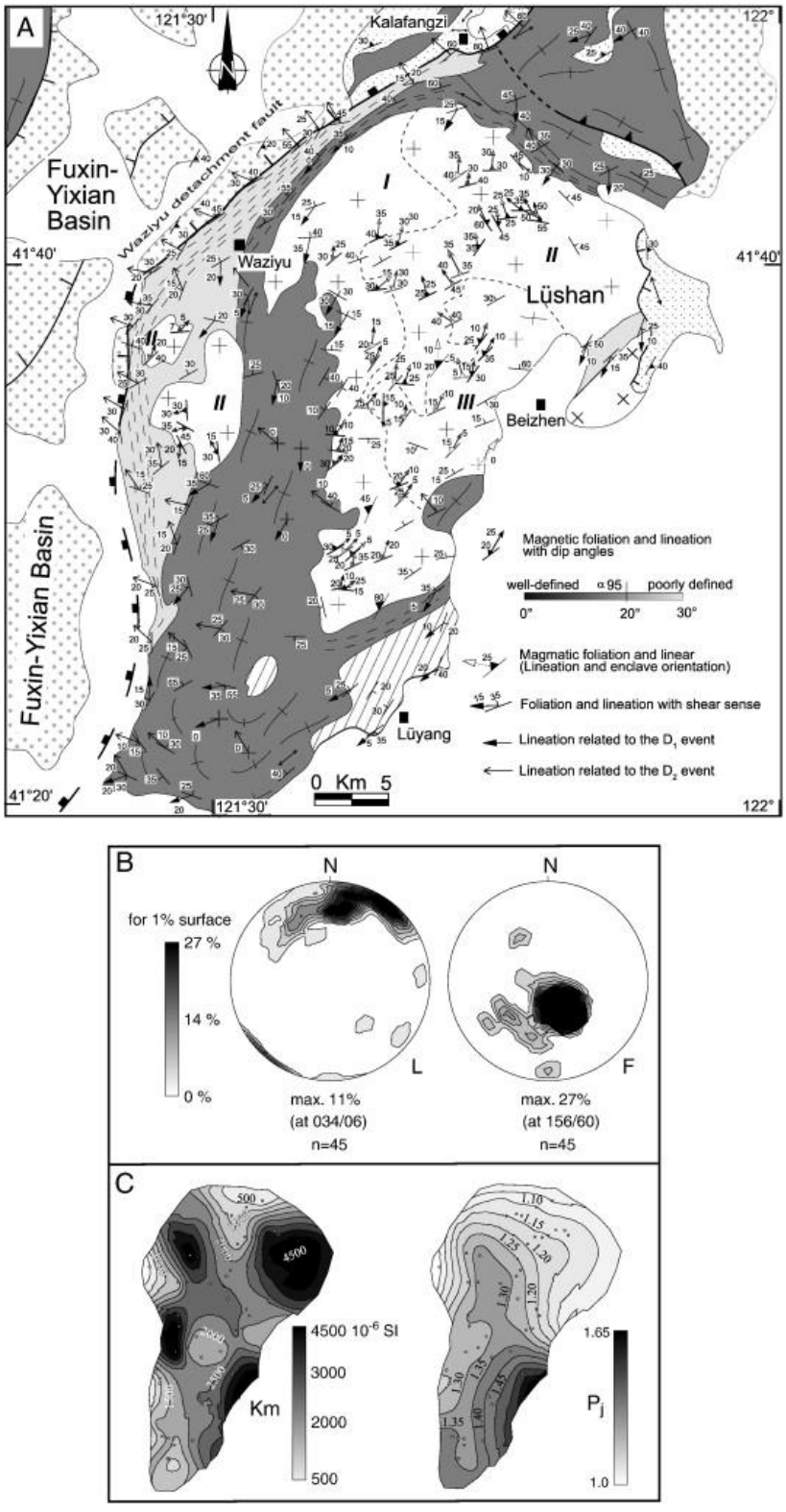

Fig. 9. (A) Combined magnetic and field structure fabrics map of the Yiwulüshan massif. Symbols and captions are the same as in Fig. 1. (B) Equal-area projections (lower hemisphere) showing density contours of individual AMS axes of the Lüshan pluton (D; F: foliation pole, L: lineation). (C) Spatial interpolation of K_m and P_J for the Lüshan Pluton.

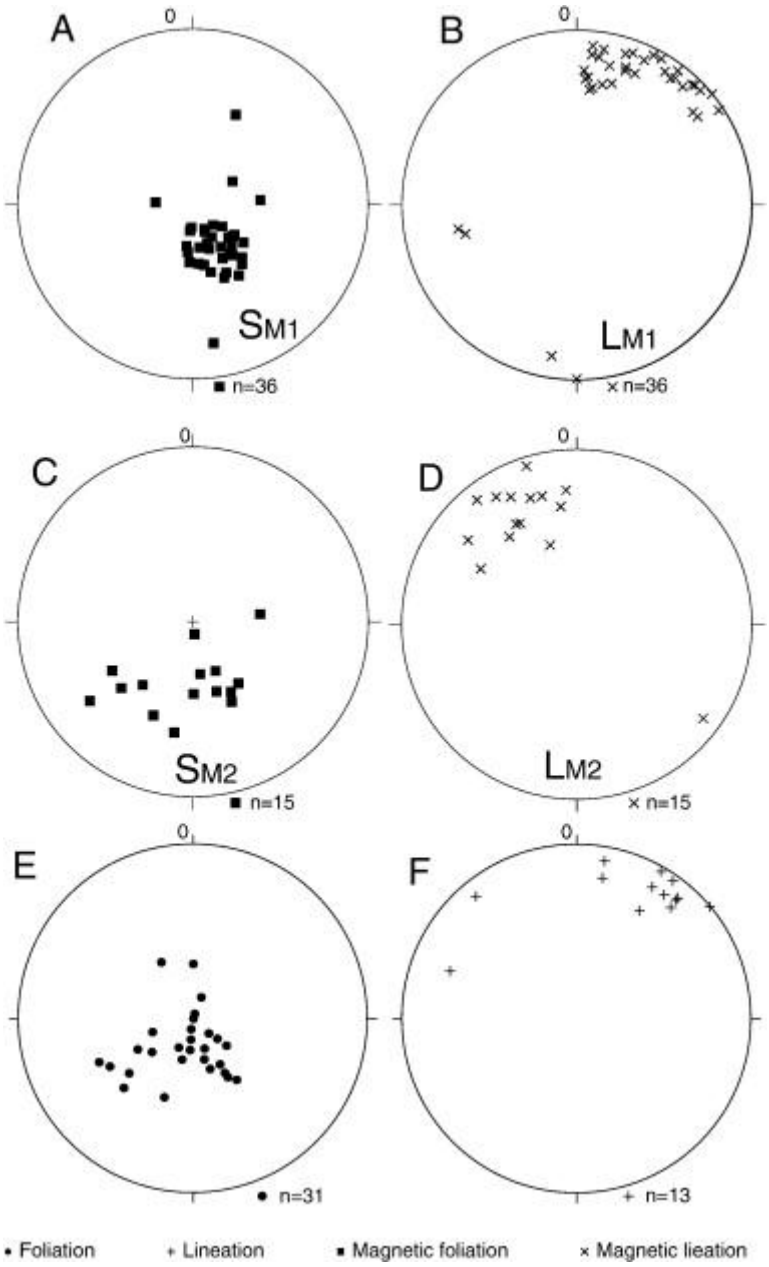

Fig. 10. Equal-area projections representing magnetic and field planar and linear structural elements of the Lüshan, Jianshilazi and Guanyindong plutons. (A) to (D) Magnetic fabrics with L_M (magnetic lineation corresponding to K_1) and S_M (pole of magnetic foliation corresponding to K_3). (E) and (F) Foliations and lineations measured in the field.

Fig. 9C shows a kriging interpolation at the Lüshan pluton-scale for the magnetic susceptibility, K_m, and the corrected anisotropy degree, P_J. It seems that no spatial distribution for K_m can be demonstrated. However, P_J values clearly indicate a regular spatial variation, with increasing values from N to S. This latter observation is coherent with the field structural and microstructures observations (Fig. 1 and Fig. 4).

3.4. Gravity modeling

Gravity data analysis and modeling have already proven their efficiency for bulk architecture and particularly for the study of plutons (e.g. [Joly et al., 2009] and [Charles et al., 2011]). In the Yiwulüshan massif, available gravity data from the Chinese regional gravity surveying (1:200,000) have been used to model the bulk crustal scale architecture of the Lüshan pluton and Shishan pluton.

The original gravity data spaced more precise than one station per 2 km ∗ 2 km (LNBGMR-GM, 1989). The gravity anomaly was acquired by calculating original data with respect to the theoretical value of gravitational acceleration of Hayford-1930 ellipsoid (Torge, 2001). Standard free air, plateau and terrain corrections were performed during this surveying ([LNBGMR-GM, 1989] and Ministry of Geology and mineral resources of People's Republic of China (MGMR), 1993). The data were measured and treated in ± 0.039 mgal for the Bouguer anomaly (MGMR, 1993). Using the complete Bouguer anomaly of those gravity stations, we interpolated the original data to a 50 m ∗ 50 m grid in the Yiwulüshan massif area (Fig. 11A). A significant negative gravity anomaly is located in the northern part of the massif, whereas the surrounding gneissic monzogranite and gneissic plagio-amphibolite show rather high gravity values in both north and south of the massif. A relative negative gravity anomaly is also revealed in the west of the massif, which was produced by the weak-density Fuxin–Yixian Mesozoic basin. If comparing the Lüshan and Shishan plutons, the higher negative anomalies are localized at the north part of the Lüshan pluton, which is consistent with the thicker low-density monzogranite. Along the margin of the Lüshan and Shishan plutons, iso-contours of Bouguer anomaly strike subparallel to the geological boundaries. However, these iso-contours have a clear displace at the north and south boundary of the Lüshan pluton. To estimate the geometry of the Yiwulüshan massif, a NNE–SSW gravity profile has been extracted (Fig. 11B) and two dimensional (2D) gravity modeling has been performed using the Geosoft-GM-SYS software (e.g. [Joly et al., 2009] and [Charles et al., 2011]). For this study, average densities were derived from laboratory measurements (Table 2) and the surfaces of deep geometries were constrained by available geological maps and our own field observations. Densities of different lithologies (Fig. 1) have been estimated as follows: (1) 2.63 g/cm^3 for granitic rocks of Lüshan and Shishan plutons (monzogranite, granodiorite, adamellite and tonalite), (2) 2.74 g/cm^3 for surrounding rocks of plutons (micaschist, orthogneiss and gneissic monzogranite), and (3) 2.62 g/cm^3 for metamorphosed sedimentary cover (micaschist, marble, phyllite and metapelite). The modeling assumed that the Moho and deeper structure surface are flat (Chen et al., 2009), therefore the shallow density of different units (0–10 km in depth) is the main contribution to the Bouguer anomaly in this kind of scale (Charles et al., 2011). We had adjusted the form of boundaries to fit the measured gravity Bouguer anomaly. The result reveals a possible feeder zone to the north of the Lüshan pluton and the development of a tabular shape to the south.

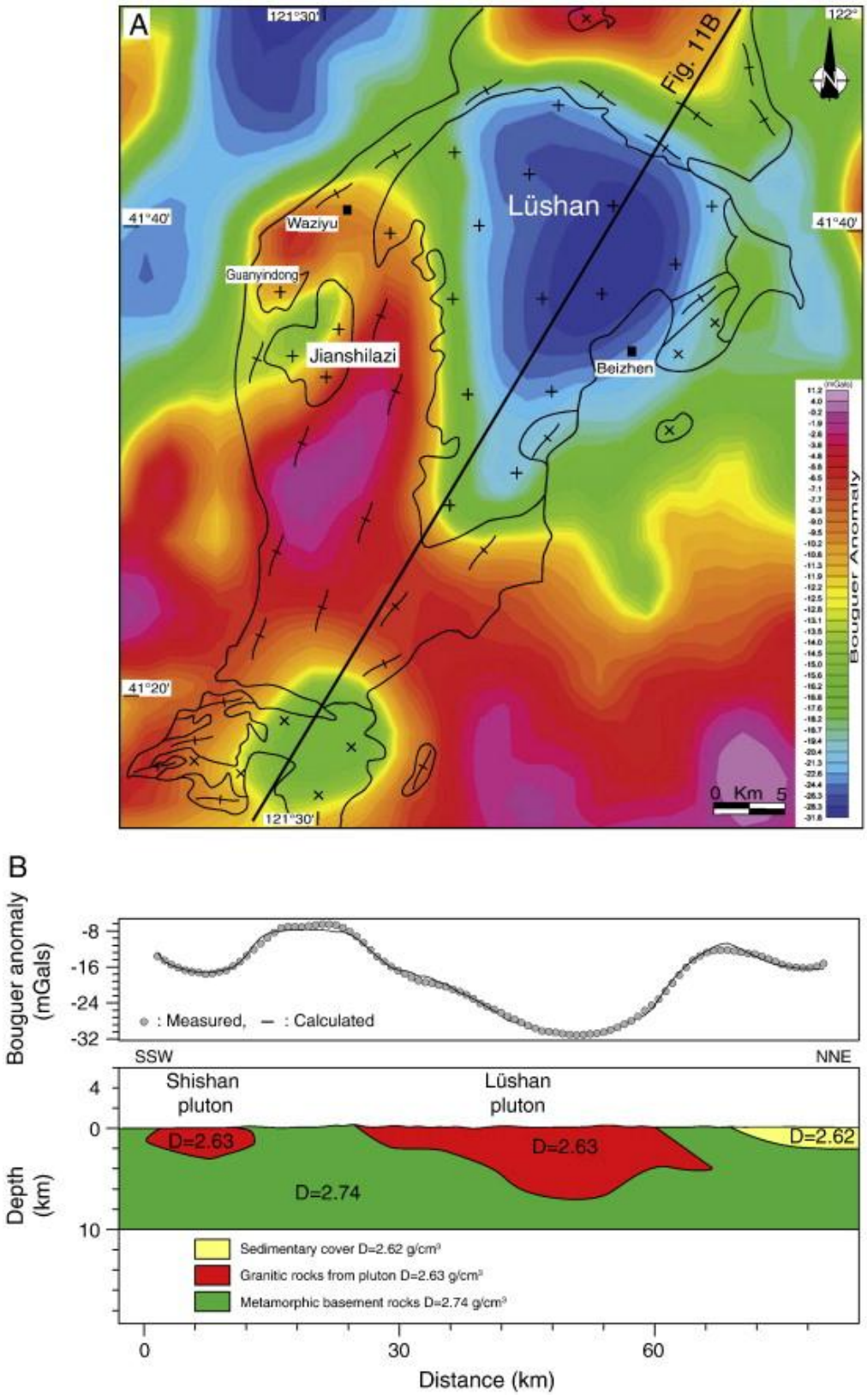

Fig. 11. (A) Bouguer anomaly map of the Yiwulüshan massif (values in mgal). (B) Measured Bouguer anomaly cross-section with modeling of deep structures geometry. Densities were estimated according to the previews work of Linglong massif (Charles et al., 2011).

Table 2. The measurement of the density from different rocks of the Yiwulüshan massif.

Sample no.	Lithology	Density of measurement	Density for modeling
Y1	Monzogranite	2.65	2.63 (granite of pluton)
Y28	Monzogranite	2.62	
Y29	Monzogranite	2.63	
Y35	Granodiorite	2.65	
Y54	Monzogranite	2.63	
Y73	Monzogranite	2.64	
Y75	Biotite granite	2.64	
YU7	Monzogranite	2.62	
YU18	Biotite–monzogranite	2.64	
YU20	Biotite–monzogranite	2.63	
YU37	Biotite–monzogranite	2.64	
Y5	Monzogranite	2.60	2.62 (sedimentary covers)
Y45	Argillaceous limestone	2.58	
Y47	Meta-volcanic rocks	2.65	
Y4	Amphibolite	2.75	2.74 (basements)
Y8	Biotite schist	2.74	
Y10	Sericite–quartz–schist	2.72	

4. Discussion

4.1. Origin(s) of magnetic fabrics

The micro-structural study of geographically representative thin-sections of samples does not reveal primary magmatic fabrics (Fig. 3). Indeed, most of the studied samples seem to have experienced a post-solidus deformation (Fig. 3 and Fig. 4). The AMS measurements may confirm this observation since more than 70% of studied sites reveal P_J values higher than 1.2, which is usually considered as the threshold of the deformation in post-solidus state (Fig. 7A and C; Tarling and Hrouda, 1993). P_J value can be related to the ferromagnetic mineral contents, i.e. high P_J value corresponding to high concentration of magnetite (e.g. Borradaile and Henry, 1997). However, it seems that is not the case for this study since no evident correlation between P_J and K_m is shown (Fig. 7C). Moreover, no evident link can be established between the granite types and P_J values or microstructure (Fig. 1, Fig. 3 and Fig. 9C). However, microstructures and P_J values show a regular spatial variation with a southward increase of intensity (Fig. 4 and Fig. 9C). Thus, we may suggest that the post-solidus deformation of the pluton is strong enough to reset a magnetic fabric related to magma emplacement and allows the granitoids to acquire new magnetic fabrics. If this hypothesis is correct, the next critical questions concern the spatial distribution of P_J values,

spatial correlation between magnetic and tectonic fabrics as well as the ages of two sub-populations of magnetic lineations.

4.2. Magnetic vs. tectonic fabrics

As described in Lin et al. (2012) and discussed above, the Yiwulüshan massif experienced significant deformations after granite crystallization, and these deformations are visible along the contact zones and on few limited exposures in the massif. Figs. 9A and 10 show both magnetic fabrics and structural signatures observed in the field where the deformation is macroscopically visible. In the Lüshan, Jianshilazi and Guanyindong plutons, two groups of magnetic lineations have been discriminated: L_{M1} exhibits a NE–SW direction with a mean around N34°E (Fig. 10B) and the L_{M2} has a NW–SE direction with a mean around N335°E (Fig. 10D). Even the L_{M2} have a little variation, these two groups of magnetic lineations are globally consistent with structural observations in the Yiwulüshan massif (Fig. 5 in Lin et al., 2012, Part I). This means that these two groups of magnetic lineations correspond to the D_1 and D_2 events which are also observed within the host-rock of plutons. Thus, the two different magnetic fabrics within the Lüshan, Jianshilazi and Guanyindong plutons were recorded during early Late Jurassic–Early Cretaceous (around 141 Ma) compressional event and Early Cretaceous (around 126 Ma) extensional event.

The comparison reveals a remarkable consistence between magnetic and tectonic fabrics all over the Lüshan pluton, with a rather flat and NW dipping foliations, associated with flat and N to NNE plunging lineations (Fig. 10). This result implies that when the deformation is strong enough, structural observations can be considered as representative for tectonic interpretation and AMS investigation may offer a better coverage of the study area with statistically more precise measurements. One surprising result from our AMS study concerns the group of magnetic fabric directions in the northeastern part of the pluton, which is seldom observed in the field (Fig. 9A). This group shows a NW plunging magnetic lineation, being well-distinguished from the N to NE general trend (Figs. 9A and 10). In fact, no apparent deformation could be directly observed in the field corresponding to this group of magnetic lineations. These statistically well-grouped and well-distinguished magnetic fabrics may indicate that the study area may have experienced a different deformation in both space and/or time with respect to the remaining main part of the Lüshan pluton (see Discussion). This encouraging result puts forward the utility of the AMS method as an efficient petrofabric tool, especially for the weakly deformed granitic rocks. Moreover, AMS measurements demonstrate much more precise and better grouped fabric orientations than the traditional geological measuring during the field work (Figs. 9A and 10).

4.3. Age(s) of magnetic fabrics

The detail analyses have been presented in Lin et al. (2012), so, a brief summary is only made here. In order to reveal the ages of polyphase tectonics, nine samples have been collected during the field work, and have been dated by conventional $^{40}Ar/^{39}Ar$ method using a step-heating procedure. Amphibole, biotite, muscovite and K-feldspar have been chosen from mylonitized micaschist, orthogneiss, and plagio-amphibolite involved into the D_1 and D_2 tectonic phases (Fig. 2). $^{40}Ar/^{39}Ar$ dating of these mylonitic samples gives two groups of ages. The earlier group, from the amphibole, biotite and K-feldspar of the mylonitic tonalitic orthogneiss, monzogranite, amphibolite and micaschist at the southern and eastern parts of the massif indicate ages ranging from 151 to 137 Ma, with a statistical peak around 141 Ma (Lin et al., 2012). The later stage, between 129 and 97 Ma, has a statistical peak around 126 Ma

from the mylonitic orthogneiss, monzogranite, plagio-amphibolite and micaschist at the western and north-western parts of the Yiwulüshan massif along the Waziyu detachment fault (Lin et al., 2012). These two different group ages can be considered to be the closer to the deformation ages of D_1 and D_2 events, respectively.

It seems clear that the Yiwulüshan massif has experienced two phases of deformation after its crystallization at ca. 160 Ma, the earlier one occurred at ca. 141 Ma and the later one at ca. 126 Ma. As described above, two groups of structural domain of the distribution of magnetic fabrics may be defined, the first group covers the major area, and the second one occupies only the northeastern part of the Lüshan pluton (Figs. 9A and 12).

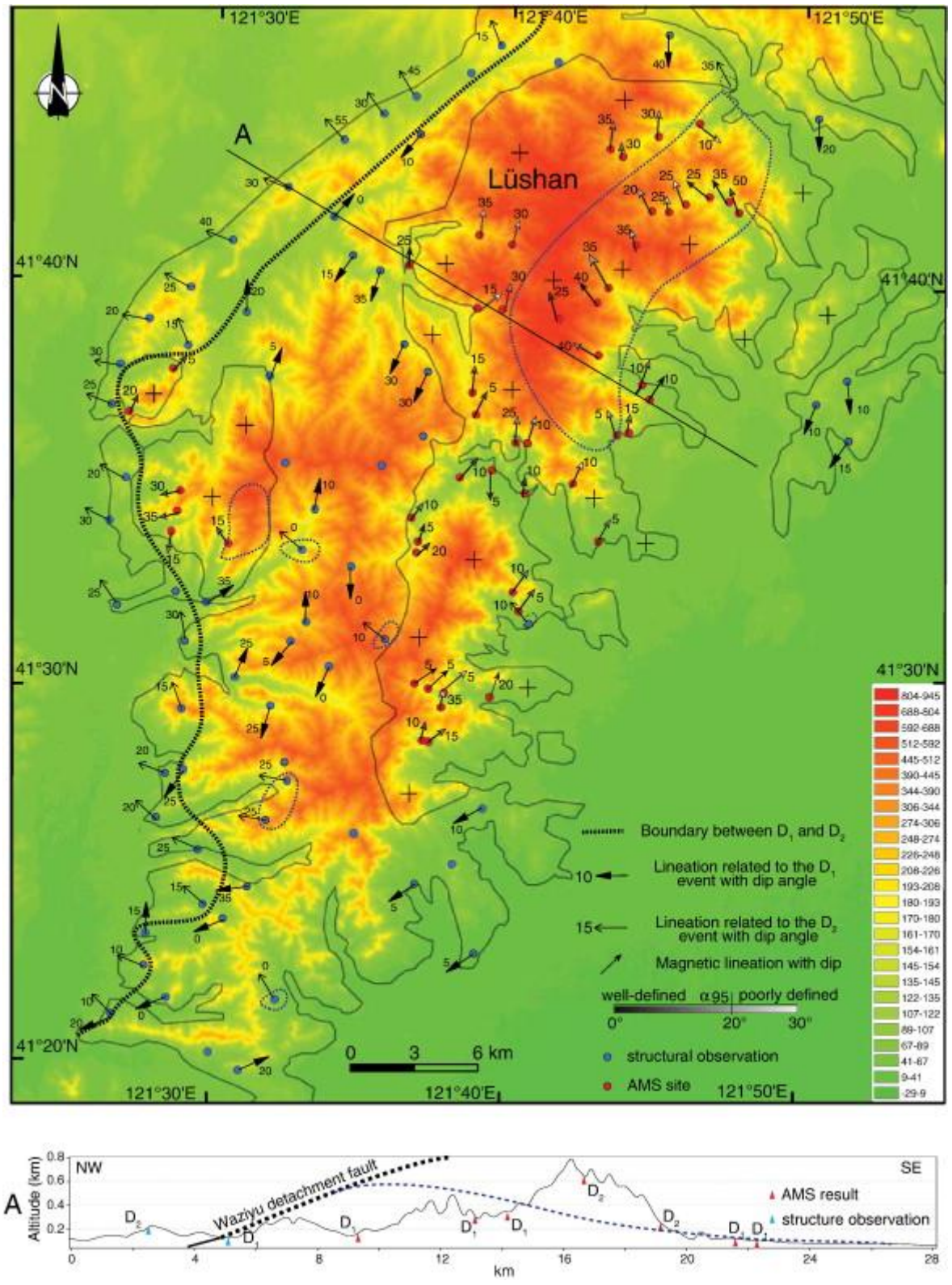

Fig. 12. Digital elevation model of the Yiwulüshan massif and surrounding areas, with magnetic and field lineations map corresponding to the different tectonic stages D_1 and D_2. The boundary between D_1 and D_2 events (blue dash line) has been drawn according to the topography (the sediment of the Quaternary fluviatile had been taken into consideration for the geological boundary to correspond the topography). (For interpretation of the references to color in this figure legend, the reader is referred to the web version of this article.)

4.4. Tectonic interpretation and evolution

Two groups of magnetic lineations have been identified (Figs. 9a and 12). By microstructural and magnetic mineralogy studies, magnetic fabrics of both groups may be considered as secondary ones, meaning that these fabrics are acquired in post-solidus state after the crystallization of the pluton. Moreover, integrating detailed structural and geochronogical analyses made in Lin et al. (2012), magnetic lineation orientations of these two groups are consistent with those structurally measured in the field, with a N to NE trending corresponding to D_1 at ca. 141 Ma and the NW trending lineation corresponding to D_2 at 126 Ma (Fig. 2 and Fig. 12). The fast cooling periods and statistical peaks could reflect these two different tectonic events (Fig. 2 and Lin et al., 2012). Combining both tectonic and magnetic fabrics (blue and red dots, respectively in Fig. 12), the D_1 (compressional) tectonic can be essentially observed in the main core of the Yiwulüshan massif, whereas the D_2 (extensional) tectonics mainly localized on the western border (along the Waziyu detachment fault) and northeastern part of the Lüshan pluton. The younger D_2 extensional event on the western border of the massif is well expressed along the Waziyu detachment fault with mylonitization of monzogranitic orthogneiss, micaschist, and plagio-amphibolite (see detailed description in Part I, Lin et al., 2012). Nevertheless, there is an issue on how to explain the D_2 tectonic observed within the Lüshan pluton without the visible detachment fault separating D_1 and D_2 phases. According to our field observations and AMS study, one possible hypothesis can be made as follows. During the D_1 event at ca. 141 Ma, the whole massif experienced a compressional tectonic and recorded the N(E)–S(W) oriented and weakly inclined lineation. Moreover, the major kinematics indicates a southward or southwestward shearing which seems to be consistent with the pluton geometry constrained by gravity modeling (Fig. 11). The later extensional D_2 tectonics is marked by the Waziyu detachment fault, which separates the Mesozoic sedimentary cover from the basement (see Fig. 3b in Part I, Lin et al., 2012). Due to the continuous extensional tectonics leading exhumation of the whole Yiwulüshan massif and consequent erosion, this detachment fault could be only traced along its western margin (thick blue line in Fig. 12) where it was deeply buried. An attempt to estimate the deformation limit between D_1 and D_2 tectonic features within the massif has been shown in Fig. 12. The dashed blue line, crossing the massif east-westwards, is suggested to separate these two events. For the space where this line is in air, the lower part recorded only the D_1 event and the upper part, which is affected by the D_2 tectonic, may well be eroded. Our AMS results show, therefore, both D_1 and D_2 (Figs. 9a and 12). For the space where the dashed blue line crosses the massif, the AMS sampling comes from the upper part, which has been deformed by D_2 but not yet eroded, and naturally preserves the D_2 fabrics (Fig. 12). It is worthy to emphasize here that the northeastern part of the massif where the D_2 is recorded is located also under the detachment because this latter is not observed in the field, and this zone is stretched by the detachment during D_2 event with relatively weak deformation. Indeed, no visible deformation can be observed in this area (except two points of field observations at the south and southwest of this area; Fig. 12). Further, petrofabric study and corrected anisotropy degree P_J values show also the presence of weak deformation in this area.

Combining the structural and geochronological analyses of the Yiwulüshan massif with the AMS and petrofabric studies provided in this paper, the following tectonic scenario may be drawn for the polyphase deformation in the Yiwulüshan massif during late Mesozoic times (Fig. 13).

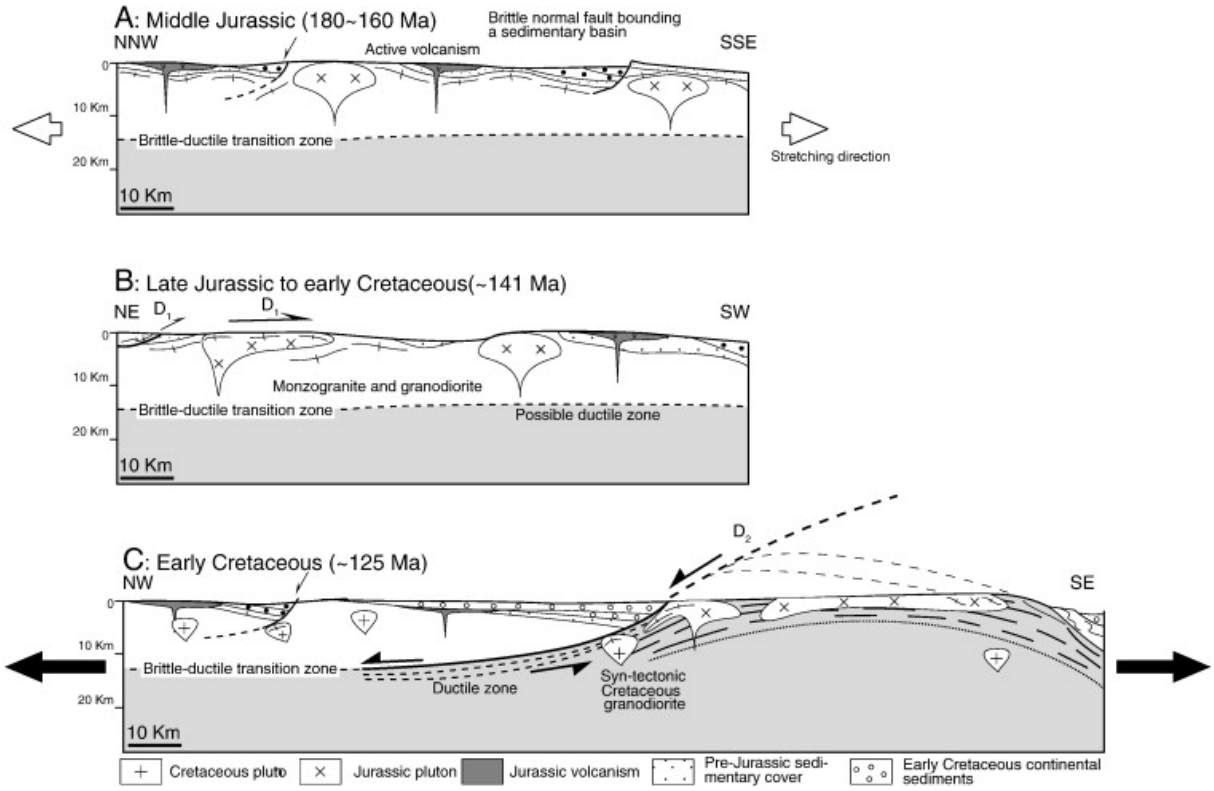

Fig. 13. Tectonic evolution of the Yiwulüshan massif, from compression to extension. (A) Lower to Middle Jurassic (180–160 Ma): extensional tectonics induced volcanism and volcano-sedimentary deposits in half-graben basins in the hanging-wall, and monzogranitic plutonism in the footwall. Up to now, ductile shearing is not documented by our field study. (B) Late Jurassic to Early Cretaceous (~ 141 Ma): a top-to-the-S(W) compressional tectonics (regional D_1 event) developed in the Yiwulüshan massif. (C) Early Cretaceous (~ 125 Ma): a significant NW–SE crustal stretching (D_2 event) occurred as documented throughout East Asia. In the hanging-wall, the half-graben is infilled by continental red-beds. In the footwall, the dome exhumes, and the Jurassic monzogranitic plutons (i.e. Lüshan, Jianshilazi and Guanyindong) underwent plastic deformation.

From Lower to Middle Jurassic (around 180–160 Ma), the Yinshan–Yanshan belt was affected by a NNW–SSE regional crustal stretching ([HBGMR, Hebei Bureau of Geology and Mineral Resources, 1989], [LBGMR, Liaoning Bureau of Geology and Mineral Resources, 1989], [He et al., 1998], [Davis et al., 2001] and [Davis et al., 2009]). This extensional tectonics induced ENE–WSW trending middle Jurassic basins (He et al., 1998; Fig. 15 of Part I, Lin et al., 2012), volcanic rocks (Zhao et al., 2004) and granitic intrusions (Wu et al., 2006). In the Yiwulüshan massif, the Lüshan, Jianshilazi and Guanyindong plutons which are coeval to this extensional event do not exhibit clear deformation related to this tectonic stage in the field. Therefore, despite the lack of direct structural constraints of ductile deformations, we suggest that the Lower to Middle Jurassic might represent the onset of continental crustal extension in the Yiwulüshan massif (Fig. 13A). From Late Jurassic to Early Cretaceous, a compressional event with a top-to-the-south to southwest sense of shear

was well documented in the Yinshan–Yanshan belt. Indeed, the Gubeikou high-angle brittle reverse fault is dated between 148 and 132 Ma (Davis et al., 2001). Besides this, at the north of Beijing city, the Miyun and Sihetang ductile thrusts in the Yunmengshan massif are dated to 143 Ma to 127 Ma ([Davis et al., 1996] and [Davis et al., 2001]). This top-to-the-south to southwest thrusting stage presented in the Yiwulüshan massif is comparable with above described structures (Fig. 13B; [Davis et al., 1996] and [Davis et al., 2001]). From the view of the entire Yinshan–Yanshan belt, this compressional deformation looks like a regional tectonic event. Conversely, during the Early Cretaceous (around 126 Ma), a NW–SE ductile extensional shearing widely developed throughout the East China ([Davis et al., 1996], [Davis et al., 2001], [Darby et al., 2004] and [Lin et al., 2011b] and reference therein). At that time, sedimentary basins widened and Jurassic plutons started to be deformed under post-solidus conditions (Fig. 12 and Fig. 13C). The Yiwulüshan massif is the easternmost extensional dome recognized in the Yinshan–Yanshan belt. The Early Cretaceous extensional tectonics is subdivided into D_2, D_3 and D_4 events, which are responsible for the final formation of the Yiwulüshan massif (Fig. 13C). In fact, the NW–SE trend of the maximum stretching is a general feature of East Asian continent during late Mesozoic. Geodynamic cause(s) for late Mesozoic extension in East Asia is still highly debated and is partly discussed in Lin et al. (2012).

5. Conclusions

In order to better understand the Late Mesozoic tectonic evolution in East Asia, the Yiwulüshan massif has been chosen as the target of investigation as it has experienced polyphase tectonics. To recognize deformation features, especially on the weakly deformed granitic plutons, and the architecture of this massif, the anisotropy of magnetic susceptibility (AMS) and gravity modeling have been carried out, coupling with structural and geochronological studies (Lin et al., 2012). Magnetic fabric has been characterized for this collection by microscopic observations and AMS measurements, implying that the magmatic fabrics have been reset by post-solidus deformations of plutons. A relatively gently NW dipping magnetic foliation has been identified with two distinct groups of magnetic lineations of 34° and 335° orientations, namely L_{M1} and L_{M2}, relatively. Integrating new geochronological results presented in Lin et al. (2012), these two groups of magnetic lineations correspond to two successive tectonic events, D_1 and D_2, which are also observed within the host-rock of the plutons, i.e., the early Late Jurassic–Early Cretaceous D_1 compressional event at around 141 Ma and the Early Cretaceous D_2 extensional event at around 126 Ma. Gravity modeling reveals a southward thinning of the massif with a possible feeder zone rooted in the northern part of the massif. This phenomenon is consistent with the spatial distributions of corrected anisotropy degree, P_J, and microstructures.

The outstanding advantage of AMS method is that the magnetic fabrics observed on the pluton are highly consistent with the fabrics acquired in their country rocks. This advantage becomes much more important when the granitic rocks are severely weekly deformed. As a result, this method is considered as a complementary petrofabric tool for finite strain analysis, since planar and linear structural elements are not always macroscopically observable in the field.

Integrating all results from structural observation, geochronological investigation, AMS measurements and gravity modeling, two tectonic phases have been identified in the Yiwulüshan massif, following the Jurassic (180–160 Ma) magmatism in the Yinshan–Yanshan area. The early one comprises a Late Jurassic–Early Cretaceous (~ 141 Ma)

compressional event with a top-to-the-south to southwest sense of shear. The second one is an Early Cretaceous (~ 126 Ma) NW–SE ductile extensional shearing. At that time, sedimentary basins widened and Jurassic plutons started to be deformed under post-solidus conditions. In fact, the NW–SE trend of the maximum stretching direction is a general feature of East Asian continent during late Mesozoic.

Acknowledgments

Field and laboratory expenses have been supported by NSFC (90714007, 40872142). Sincere thanks are presented to two anonymous reviewers and Guest Editor of this special issue for their constructive suggestions.

References

Andryushchenko et al., 2010 S.V. Andryushchenko, A.A. Vorontsov, V.V. Yarmolyuk, I.V. Sandimirov Evolution of Jurassic–Cretaceous magmatism in the Khambin volcanotectonic complex (western Transbaikalia) Russian Geology and Geophysics, 51 (2010), pp. 734–749

Archanjo et al., 1995 C.J. Archanjo, P. Launeau, J.L. Bouchez Magnetic fabrics vs magnetite and biotite shape fabrics of the magnetite-bearing granite pluton of Garmeleiras (northeast Brazil) Physics of the Earth and Planetary Interiors, 85 (1995), pp. 63–75

Bell and Johnson, 1989 T.H. Bell, S.E. Johnson Porphyroclast intrusion trails: the key to orogenesis Journal of Metamorphic Geology, 3 (1989), pp. 109–118

Bingham, 1964 Bingham, C., 1964. Distributions on the sphere and on the projective plane. PhD thesis, Yale University, New Haven.

Borradaile and Gauthier, 2003 G.J. Borradaile, D. Gauthier Emplacement of an Archean gneiss dome, northern Ontario, Canada: inflation inferred from magnetic fabrics Tectonics, 22 (2003), p. 1011 http://dx.doi.org/10.1029/2002TC001443

Borradaile and Henry, 1997 G.J. Borradaile, B. Henry Tectonic applications of magnetic susceptibility and its anisotropy Earth Science Reviews, 42 (1997), pp. 49–93

Bouchez, 2000 J.L. Bouchez Anisotropie de susceptibilité magnétique et fabrique des granites Comptes Rendus de l'Académie des Sciences, 330 (2000), pp. 1–14

Charles et al., 2011 N. Charles, C. Gumiaux, R. Augier, Y. Chen, W. Lin, R. Zhu Metamorphic core complex vs. synkinematic pluton in continental extension setting: insights from key structures (Shandong Province, eastern China) Journal of Asian Earth Sciences, 40 (2011), pp. 261–278

Chen et al., 2009 L. Chen, C. Cheng, Z.G. Wei Seismic evidence for significant lateral variations in lithospheric thickness beneath the central and western North China Craton Earth Planetary Science Letters, 286 (2009), pp. 171–183

Chough and Sohn, 2010 S.K. Chough, Y.K. Sohn Tectonic and sedimentary evolution of a Cretaceous continental arc–backarc system in the Korean peninsula: new view Earth-Science Reviews, 101 (2010), pp. 225–249

Chough et al., 2000 S.K. Chough, S.T. Kwon, J.H. Ree, D.K. Choi Tectonic and sedimentary evolution of the Korean Peninsula: a review and new view Earth Science Reviews, 52 (2000), pp. 175–235

Cui and Wu, 1997 S. Cui, Z. Wu On the Mesozoic and Cenozoic intracontinental orogenesis of the Yanshan area, China Y. Zheng (Ed.) *et al.*, Proceedings of the 30th International Geological Congress 14, VSP, Utrecht, The Netherlands (1997), pp. 277–292

Cui et al., 2002 S.Q. Cui, J.R. Li, Z.H. Wu, M.C. Yi, S.M. Shen, H.R. Yin, Y.S. Ma Mesozoic and Cenozoic Intracontinental Orogenesis of the Yanshan Area Geological Publishing House, Beijing (2002), pp. 261–279 (in Chinese with English abstract)

Daoudene et al., 2011 Y. Daoudene, G. Ruffet, A. Cocherie, P. Ledru, D. Gapais Timing of exhumation of the Ereendavaa metamorphic core complex (north-eastern Mongolia) — U–Pb and $^{40}Ar/^{39}Ar$ constraints Journal of Asian Earth Sciences (2011) http://dx.doi.org/10.1016/j.jseaes.2011.04.009

Darby and Ritts, 2002 B.J. Darby, B.D. Ritts Mesozoic contractional deformation in the middle of the Asian tectonic collage; the intraplate Western Ordos foldthrust belt, China Earth and Planetary Science Letters, 205 (2002), pp. 13–24

Darby et al., 2004 B.J. Darby, G.A. Davis, X. Zhang, F. Wu, S. Wilde, J. Yang The newly discovered Waziyu metamorphic core complex, Yiwulüshan, western Liaoning province, Northwest China Earth Science Frontiers, 11 (2004), pp. 145–155

Davis and Darby, 2010 G.A. Davis, B.J. Darby Early Cretaceous overprinting of the Mesozoic Daqing Shan fold-and-thrust belt by the Hohhot metamorphic core complex, Inner Mongolia, China Earth Science Frontiers, 17 (2010), pp. 1–20

Davis et al., 1996 G.A. Davis, X. Qian, Y. Zheng, H. Yu, C. Wang, T.H. Mao, G.E. Gehrels, S. Muhammad, J.E. Fryxell Mesozoic deformation and plutonism in the Yunmeng Shan: a Chinese metamorphic core complex north of Beijing, China A. Yin, T.A. Harrison (Eds.), The Tectonic Evolution of Asia, Cambridge University Press, New York (1996), pp. 253–280

Davis et al., 1998 G.A. Davis, C. Wang, Y. Zheng, J. Zhang, C. Zhang, G.E. Gehrels The enigmatic Yinshan fold-and-thrust belt of northern China: new views on its intraplate contractional styles Geology, 26 (1998), pp. 43–46

Davis et al., 2001 G.A. Davis, Y. Zheng, C. Wang, B.J. Darby, C. Zhang, G.E. Gehrels Mesozoic tectonic evolution of the Yanshan fold and thrust belt, with emphasis on Hebei and Liaoning provinces, northern China ,in: M.S. Hendrix, G.A. Davis (Eds.), Paleozoic and Mesozoic Tectonic Evolution of Central and Asia: From Continental Assembly to Intracontinental Deformation, Geological Society of American Memoirs, 194 (2001), pp. 171–194

Davis et al., 2009 G.A. Davis, J.F. Meng, W.R. Cao, X.Q. Du Triassic and Jurassic tectonics in the eastern Yanshan Belt, North China: insights from the controversial Dengzhangzi Formation and its neighboring units Earth Science Frontiers, 16 (2009), pp. 69–86

Deng et al., 2004 J. Deng, X. Mo, H. Zhao, Z. Wu, Z. Luo, S. Su A new model for the dynamic evolution of Chinese lithosphere: 'continental roots-plume tectonics' Earth Science Reviews, 65 (2004), pp. 223–275

Du et al., 2007 J. Du, Y. Ma, Y. Zhao, Y. Wang SHRIMP U–Pb zircon dating of the Yiwulüshan granite in western Liaoning and its geological implications Geology in China, 24 (2007), pp. 26–33

Eggleton and Buseck, 1980 R.A. Eggleton, P.R. Buseck The orthoclase-microcline inversion: a high-resolution transmission electron microprobe study and strain analysis Contributions to Mineralogy and Petrology, 74 (1980), pp. 123–133

Erdenetsogt et al., 2009 B.O. Erdenetsogt, I. Lee, D. Bat-Erdene, L. Jargal Mongolian coal-bearing basins: geological settings, coal characteristics, distribution, and resources International Journal of Coal Geology, 80 (2009), pp. 87–104

Geng et al., 2012 Y. Geng, L. Du, L. Ren Growth and reworking of the early Precambrian continental crust in the North China Craton: constraints from zircon Hf isotopes Gondwana Research, 21 (2012), pp. 517–529

Grégoire et al., 1995 V. Grégoire, M. Saint Blanquat (de), A. Nédélec, J.L. Bouchez Shape anisotropy vs magnetic interactions of magnetite grains: experiments and application to AMS in granitic rocks Geophysical Research Letters, 18 (1995), pp. 2193–2196

Grégoire et al., 1998 V. Grégoire, J. Darrozes, P. Gaillot, A. Nédélec Magnetite grain shape fabric and distribution anisotropy vs rock magnetic fabric: a three-dimensional case study Journal of Structural Geology, 20 (1998), pp. 937–944

HBGMR, Hebei Bureau of Geology and Mineral Resources, 1989 HBGMR, Hebei Bureau of Geology and Mineral Resources Regional Geology of Hebei Province. Ministry of Geology and Mineral Resources Geological Memoirs, 15 (1989), pp. 1–741 (in Chinese with English summary)

He et al., 1998 Z.J. He, J.Y. Li, B.G. Niu, J.S. Ren A Late Jurassic intense thrusting-uplifting event in the Yanshan–Yinshan area, northern China, and its sedimentary response Geological Review, 44 (1998), pp. 407–418

Jelinek, 1978 V. Jelinek Statistical processing of anisotropy of magnetic susceptibility measures on groups of specimens Studia geophisica et geodetica, 22 (1978), pp. 50–62

Jelinek, 1981 V. Jelinek Characterization of the magnetic fabric of rocks Tectonophysics, 79 (1981), pp. 63–67

Joly et al., 2009 A. Joly, M. Faure, G. Martelet, Y. Chen Gravity inversion, AMS and geochronological investigations of syntectonic granitic plutons in the southern part of the Variscan French Massif Central Journal of Structural Geology, 31 (2009), pp. 421–443

LBGMR, Liaoning Bureau of Geology and Mineral Resources, 1989 LBGMR, Liaoning Bureau of Geology and Mineral Resources Regional geology of Liaoning Province Geological Memoirs, 14Geological Publishing House (1989), pp. 1–856 (in Chinese with English summary)

Le Goff et al., 1992 M. Le Goff, B. Henry, L. Daly Practical method for drawing a VGP path Physics of the Earth and Planetary Interiors, 70 (1992), pp. 201–204

Li et al., 1997 S. Li, F. Lu, C. Lin Evolution of Mesozoic and Cenozoic Basins in Eastern China and Their Geodynamic Background China University of Geosciences Press, Wuhan (1997), pp. 1–239 (In Chinese with English summary)

Lin et al., 2007 W. Lin, M. Faure, P. Monié, Q.C. Wang Polyphase Mesozoic tectonics in the eastern part of the North China Blocks: insights from the Liaoning Peninsula massif (NE China) ,in: M.G. Zhai, B.F. Windley, T.M. Kusky, Q.R. Meng (Eds.), Mesozoic Sub-continental Lithospheric Thinning Under Eastern Asia, Geological Society of London, Special Publications, 280 (2007), pp. 153–170

Lin et al., 2008 W. Lin, M. Faure, P. Monié, U. Schärer, D. Panis Mesozoic extensional tectonics in Eastern Asia: the South Liaodong Peninsula Metamorphic Core Complex (NE China) Journal of Geology, 116 (2008), pp. 134–154

Lin et al., 2011a W. Lin, Q. Wang, J. Wang, F. Wang, Y. Chu, K. Chen Late Mesozoic extensional tectonics of the Liaodong Peninsula massif: response of crust to continental lithosphere destruction of the North China Craton Science China Earth Sciences, 54 (2011), pp. 843–857 http://dx.doi.org/10.1007/s11430-011-4190-5

Lin et al., 2011b W. Lin, P. Monié, M. Faure, U. Schärer, Y. Shi, N. Le Breton, Q. Wang Cooling paths of the NE China crust during the Mesozoic extensional tectonics: example from the south-Liaodong peninsula metamorphic core complex Journal of Asian Earth Sciences, 42 (2011), pp. 1048–1065 http://dx.doi.org/10.1016/j.jseaes.2010.09.007

Lin et al., 2012 Lin, W., Faure, M., Chen, Y., Ji, W., Wang, F., Wu, L., Charles, N., Wang, Q. 20112012. Late Mesozoic compressional to extensional deformations in Yiwulüshan massif, NE China and their bearing on Yinshan–Yanshan orogenic belt (part I: structural and geochronological analyses). Gondwana Research, this issue.

Liu et al., 2000 J. Liu, X. Liu, S. Si, G. Li, Z. Ouyang Characterics and genesis of granitic complex in Fuxing–Jinzhou area, Liaoning province Geology–Geochemistry, 28 (2000), pp. 65–74

Liu et al., 2002 Z. Liu, Z. Xu, Z. Yang Mesozoic crustal overthrusting and extensional deformation in the Yinshan Mountains area Geological Bulletin of China, 21 (2002), pp. 246–250

Liu et al., 2005 J. Liu, G. Davis, Z. Lin, F. Wu The Liaonan metamorphic core complex, southeastern Liaoning Province, North China: a likely contributor to Cretaceous rotation of eastern Liaoning, Korea and contiguous areas Tectonophysics, 407 (2005), pp. 65–80

Liu et al., 2011 J. Liu, M. Ji, L. Shen, H. Guan, G. Davis Early Cretaceous extensional structures in the Liaodong Peninsula: structural associations, geochronological constraints and regional tectonic implications Science China Earth Sciences, 54 (2011), pp. 823–842

LNBGMR-GM, 1989 LNBGMR-GM (1989) Bureau of Geological and Mineral Resources of Liaoning Province, Gravity map, scale 1: 200,000. K-51-(21), China Ministry of Geology and Mineral Resource, Beijing.

LNBGMR-Yixian, 1970 LNBGMR-Yixian, 1970. Bureau of Geological and Mineral Resources of Liaoning Province. Geological Map of Yixian, Scale 1:200 000. China Ministry of Geology and Mineral Resource, Beijing.

Lü and Liu, 1994 J. Lü, W. Liu Features of Indosinian structures in Kalafangzi area Liaoning Geology, 12 (1994), pp. 255–262 (in Chinese)

Ma et al., 1999 Y. Ma, S. Cui, G. Wu, Z. Wu, D. Zhu, X. Li, X. Feng The structural feature of metamorphic core complex in Yiwulüshan mountains, West Liaoning Acta Geoscientia Sinica, 20 (1999), pp. 385–391 (in Chinese)

Ma et al., 2000 Y. Ma, S. Cui, G. Wu, Z. Wu, D. Zhu, X. Li, X. Feng Uplift history of the Yiwulüshan mountains in west Liaoning Acta Geoscientia Sinica, 21 (2000), pp. 245–253 (in Chinese)

Mazukabzov et al., 2006 A.M. Mazukabzov, T.V. Donskaya, D.P. Gladkochub, E.V. Sklyarov, V.A. Ponomarchuk, E.B. Salnikova Structure and age of the metamorphic core complex of the Burgutui ridge (southwestern Transbaikal region) Dokl Earth Sciences, 407 (2006), pp. 179–183

Metelkin et al., 2010 D.V. Metelkin, V.A. Vernikovsky, A.Y. Kazansky, M.T.D. Wingate Late Mesozoic tectonics of Central Asia based on paleomagnetic evidence Gondwana Research, 18 (2010), pp. 400–419

Ministry of Geology and mineral resources of People's Republic of China (MGMR), 1993 Ministry of Geology and mineral resources of People's Republic of China (MGMR) Regional gravity survey specification Geological and Mineral Resources Industry Standard of the People's Republic of China (1993)

Paterson et al., 1998 S.R. Paterson, T.K. Fowler, K.L. Schmidt, A.S. Yoshinobu, E.S. Yuan, R.B. Miller Interpreting magmatic fabric patterns in plutons Lithos, 44 (1998), pp. 53–82

Ritts et al., 2001 B.D. Ritts, B.J. Darby, T. Cope Early Jurassic extensional basin formation in the Daqing Shan segment of the Yinshan belt, northern North China Block, Inner Mongolia Tectonophysics, 339 (2001), pp. 239–258

Rochette et al., 1992 P. Rochette, M. Jackson, C. Aubourg Rock magnetism and the interpretation of anisotropy of magnetic susceptibility Reviews of Geophysics, 30 (1992), pp. 209–226

Simpson and Wintsch, 1989 C. Simpson, R.P. Wintsch Evidence for deformation-induced K-feldspar replacement by myrmekite Journal of Metamorphic Geology, 7 (1989), pp. 267–275

Su et al., 1994 C.H. Su, G.X. Lei, W.H. Liu, Z.H. Zhang Study on geological character and origin of Lüshan granite Liaoning Geology, 12 (Z1) (1994), pp. 154–164

Tarling and Hrouda, 1993 D.H. Tarling, F. Hrouda The Magnetic Anisotropy of Rocks Chapman and Hall (1993) (215 p) Torge, 2001 W. Torge Geodesy (third edition)Walter de Gruyter (2001) (416 p)

Traynor and Sladen, 1995 J.J. Traynor, C. Sladen Tectonic and stratigraphic evolution of the Mongolian People's Republic and its influence on hydrocarbon geology and potential Marine and Petroleum Geology, 12 (1995), pp. 35–52

Vergely et al., 2007 P. Vergely, M. Hou, Y. Wang, J. Mercier The kinematics of the Tan–Lu Fault Zone during the Mesozoic–Palaeocene and its relations with the North China — South China Block collision (Anhui Province, China) Bulletin de la Société Géologique de France, 178 (2007), pp. 353–365

Wang et al., 2011 T. Wang, Y. Zheng, J. Zhang, L. Zeng, T. Donskaya, L. Guo, J. Li Pattern and kinematic polarity of late Mesozoic extension in continental NE Asia: perspectives from metamorphic core complexes Tectonics (2011) http://dx.doi.org/10.1029/2011TC002896

Wong, 1929 W.H. Wong The Mesozoic orogenic movement in eastern China Geological Society of China Bulletin, 8 (1929), pp. 33–44

Wu et al., 2006 F.Y. Wu, J. Yang, Y. Zhang, X. Liu Emplacement ages of the Mesozoic granites in southeastern part of the Western Liaoning Province Acta Petrologica Sinica, 22 (2006), pp. 315–325

Wu et al., 2008 F.Y. Wu, Y.G. Xu, S. Gao *et al.* Lithospheric thinning and destruction of the North China Craton Acta Petrologica Sinica, 24 (2008), pp. 1145–1174 (in Chinese with English abstract)

Yin, 2007 Yin, G., 2007. The Tectonic Features and the Establishment's FEM Simulation of Metamorphic Core Complex in Yiwulv Mountains. M. D. Dissertation, Jinlin University, Changchun. 48pp.

Zhai and Santosh, 2011 M.G. Zhai, M. Santosh The early Precambrian odyssey of the North China Craton: A synoptic overview Gondwana Research, 20 (2011), pp. 6–25

Zhang et al., 2002 X. Zhang, T. Li, Z. Pu $^{40}Ar/^{39}Ar$ thermochronology of two ductile shear zones from Yiwulüshan, west Liaoning region: age constraints on Mesozoic tectonic events Chinese Science Bulletin, 47 (2002), pp. 697–701

Zhang et al., 2008 X. Zhang, Q. Miao, H. Zhang, S. Wilde A Jurassic peraluminous leucogranite from Yiwulüshan, western Liaoning, North China craton: age, origin and tectonic significance Geological Magazine, 145 (2008), pp. 305–320

Zhang et al., 2011a C.H. Zhang, C.M. Li, H.L. Deng, Y. Liu, L. Liu, B. Wei, H.B. Li, Z. Liu Mesozoic contraction deformation in the Yanshan and northern Taihang mountains and its implications to the destruction of the North China Craton Science China Earth Sciences, 54 (2011), pp. 798–822

Zhang et al., 2011b J. Zhang, M. Santosh, X. Wang, L. Guo, X. Yang, B. Zhang Tectonics of the northern Himalayas since the India–Asia collision Gondwana Research (2011) http://dx.doi.org/10.1016/j.gr.2011.11.004

Zhao, 1963 Z. Zhao Yanshan movement at Eastern China Chinese Journal of Geology, 3 (1963), pp. 128–138 (in Chinese with English abstract)

Zhao, 1990 Y. Zhao The Mesozoic orogenic and tectonic evolution of the Yanshan Area Geological Review, 36 (1990), pp. 1–13 (in Chinese with English abstract)

Zhao et al., 2004 Y. Zhao, G. Xu, S. Zhang, Z. Yang, Y. Zhang, J. Hu Yanshanian movement and conversion of tectonic regimes in Eastern Asia Earth Science Frontiers, 11 (2004), pp. 319–328

Zheng et al., 1998 Y.D. Zheng, G.A. Davis, C. Wang, B.J. Darby, Y.G. Hua Major thrust sheet in the Daqing Shan, Inner Mongolia, China Science in China (Series D), 31 (1998), pp. 553–560

Zhu et al., 2003 D. Zhu, X. Meng, X. Feng, Z. Shao, W. Qu, H. Zhang, H. Fu, J. Wang, M. Yang Tectonic features of metamorphic core complexes in Yiwulüshan area, Liaoning province and a dynamic analysis of rock fabrics Acta Geoscientia Sinica, 24 (2003), pp. 225–230 (in Chinese)